UNIVERSITY OF CALIFORNIA,
IRVINE

Influence of Reconfigurable Antenna Parameters on the Diversity Gain in Fading MIMO Environments: an Experimental Approach on the Spatial, Polarization and Pattern Diversity

THESIS

submitted in partial satisfaction of the requirements
for the degree of

MASTER OF SCIENCE

in Electrical and Computer Engineering

by

Alfred Grau Besoli

Thesis Committee:
Prof. Franco De Flaviis, Chair
Prof Hamid Jafarkhani
Prof. G. P. Li

2005

The thesis of Alfred Grau Besoli is approved:

Committee Chair

University of California, Irvine

2005

To my family and friends

Table of Contents

List of Tables

List of Figures

Acknowledgments

I would like to start giving many thanks to the director of my Master thesis, Prof. Franco De Flaviis, for giving me such opportunity, for his nice support during all this time and for all the knowledge that he has been able to transmit to me. Equally, I would like to thank very much Mr. Pete Balsells, for providing me a way to come to the University of California, Irvine, through the Balsells Fellowship, and for his valuable comments and initiatives.

Thanks to Prof. Roger Rangel, for his continuous and unconditional help, to Dr. Bedri A. Cetiner, for all his good advises and inspiring talks, to Prof. Lluis Jofre, for being the person that really introduced me the way towards this experience and for his help from the very beginning. I would like to thank the rest of my committee members, Prof. G. P. Li and Prof. Hamid Jafarkhani. Thanks to all the members of the lab for all their help and nice hospitality towards me, and thanks to the Electrical Engineering and Computer Science department of the Henry Samueli School of Engineering, at the University of California, Irvine, for providing me a place to conduct my Master in such a nice environment.

Special thanks to all my family and friends in Spain, French, US and Denmark for their very unconditional and unique support.

Abstract of the Thesis

Influence of Reconfigurable Antenna Parameters on the Diversity Gain in Fading MIMO Environments: an Experimental Approach on the Spatial, Polarization and Pattern Diversity

by
Alfred Grau Besoli
Master of Science in Electrical and Computer Engineering
University of California, Irvine, 2005
Prof. Franco De Flaviis, Chair

Next generation of wireless communication networks and terminals will introduce stringent requirements to satisfy: high data rate transmission over a large variety of environments. A theoretical limit for the capacity shows that those new requirements can not be satisfied using Single-Input Single-Output (SISO) schemes. A technique to overcome this limit is to employ multi-element antenna (MEA) schemes. Receiving diversity is one of those techniques and it uses multiple antennas at the receiver to improve the reception of the signal and suppress the multipath effect. In contraposition, other techniques such as space-time coding and spatial multiplexing exploit the multipath phenomena to futher increase the data rate. In general, none of those techniques

works the best in all the environments, which arises the necessity for re-configurable antennas and schemes. This work focused the research in characterize several receiving diversity schemes, in particular: space, polarization and angle diversity, to determine which one of them is the most appropriate for and indoor environment when the area of the antenna system is fixed, and determine which are the most benefitial parameters to reconfigure. Polarization diversity is seen as one of the most promising techniques to be exploited. The work conducted on this thesis, will take special interest when combining the knowledge of this research with re-configurable schemes and techniques that exploit multipath.

Chapter 1

Introduction

Next generation of wireless communication networks and terminals will introduce very stringent requirements to satisfy. In particular they will ask for high data rate capacities to be guaranteed over a large variety of environments. Those environments can be highly scattered, such as urban areas (Line-of-Sight (LOS) and Non-LOS (NLOS)), and low scattered, such as rural areas (LOS and NLOS). The requirements will need to be satisfied under two main limited resources, the bandwidth and signal power level.

It is known that capacity, bandwidth and power (or Signal to Noise Ratio (SNR)), are inter-related as stated on the Shannon equation for Single Input Single Output (SISO) communications. This equation gives us a theoretical limit in capacity for a given bandwidth and SNR. It is easy to see that the data rates requirements can't be satisfied with SISO schemes. New techniques have been developed to overcome this limitation. They are based on Multi-Element Antenna (MEA) schemes that basically allow us to further increase the capacities beyond the theoretical SISO limitation.

The multipath is a propagation phenomenon that arises in scattered environments, due to the fact that the signal transmitted, is reflected and refracted many times in his path from the transmitter to the receiver. From this scattering, multiple replicas

of the original signal, but spread in time, appear at the receiver. At the receiver, those signals can interfere constructive or destructively, and the resultant is a rapidly varying signal in which its envelope suffers very fast fading and makes the reception very difficult. Traditionally, in SISO communications, channel encoding techniques and equalization are used together to overcome this undesired fading by introducing some redundancy on the transmitted signal. However, this redundancy is translated in lower channel efficiency. MEA configurations together with Multiple Input Multiple Output schemes, allows to obtain this redundancy from the scattering characteristics of the communication channel itself, and hence no redundancy needs to be included at the transmitted signal, with no expenses in terms of efficiency.

Receiving diversity is one of those new MEA techniques referred above, and can be classified as a Single Input Multiple Output (SIMO) communication scheme. Receiving diversity consist in using multiple antennas at the receiver to mitigate the multipath phenomena and increase the SNR. Beamforming, spatial multiplexing are other technique that exploit the multipath phenomena instead of trying to avoid it, and those are also base on MEA schemes in either the transmitter and receiver. Space-time codes are used to exploit the spatial dimention of the channels to further increase the data rate or the diversity order.

With the introduction of MEA communication schemes, the Shannon equation needed to be extended to the Multiple Input Multiple Output (MIMO) communications case.

In general, none of those techniques works the best in all the environments, which arises the necessity for re-configurable antennas and schemes that can adapt to all the environments to satisfy the new requirements in any circumstance or place. At this point is where the research conducted on this thesis plays a role. On this work, a experimental electromagnetic characterization of several receiving diversity techniques (spatial, polarization and pattern) have been conducted to figure out which one is the most appropriate technique and scheme when the area reserved for the antenna system is fixed, in an indoor environment. The area reserved for the antenna system in mobile terminals is limited and hence is an expensive resource. Further-

more, an optimization of the area reserved for the antenna system need to be done. This necessity is emphasized by the fact that receiving diversity techniques employ MEA schemes, which further increase the total area for the antenna system. Antenna miniaturization and receiving diversity scheme optimization are then some of the key points for reducing the area reserved to the antenna system.

The work presented on this thesis is a experimental approach to the investigation of antenna diversity and how the antennas can be reconfigured to improve signal reliability. Micro-electro-mechanical systems is a key technology to implement such capabilities. In addition, simulations of a true realistic MIMO channel are complex and difficult to contrast with a real environment, arising the necessity for an experimental work to truly characterize the channel and scheme characteristics. Common not assumed issues in such models are:

- Cross-polarization coupling.
- Different path losses among different polarizations.
- Different CDF of the signal among different polarizations.

The information obtained on this research arises the interest to its application on MIMO re-configurable schemes. Re-configurable schemes are also of great interest since they introduce the possibility to use single antenna schemes with the capacity to work as multi-antenna schemes but occupying less area for the antenna system. They also arise the possibility to further overcome the limitations of MIMO systems, by including re-configurable capabilities in pure electromagnetic aspects of the wireless channel, such as antenna separation and the polarization.

Chapter 2

Objectives

So far, various combinations of spatial, polarization and pattern receiving diversity techniques have been considered for its use at the mobile handset, however, little research has attempted to isolate the effects of spatial, polarization and pattern diversity and study them under the same radiating characteristics. Also, little attempt has been done in investigating efficient ways to reconfigure the antennas. To reach this objective we first characterize the performance of several receiving diversity techniques and schemes, at 2.45GHz, when the area occupied by the antenna system is fixed and the same type of radiating antenna elements are used. That is: firstly, the number of antennas on each antenna setup has been fixed, because in fact, the performance of MIMO systems is inherently related with the number of antennas being used at the same time; secondly, the type of radiating antenna element has been fixed in order to compare the different antenna setups in a fair manner.

More in deep, objectives of this work are the following:

1. To study the effect of the mutual coupling in the diversity gain.
2. To study the effect of using different types of polarization in both the transmitter and receiver, such as circular or linear, on the diversity gain.

3. To study the effect of the orientation of the antenna system, that is, vertical or horizontal disposition of the antennas, on the diversity gain, in order to quantify the vertical and horizontal multipath component of an indoor channel.

4. To study the benefits from combining several diversity techniques.

5. To study the effects of power imbalance and correlation coefficient in the diversity gain.

6. To investigate the best configuration for size reduction purposes while preserving an acceptable level of diversity.

7. To investigate the most beneficial parameters (distance between antennas, scheme orientation, polarization, and type of antenna diversity) in the antennas and arrays from the reconfigurability perspective. The idea is to obtain such information for its future application in Multiple-Input Multiple-Output reconfigurable systems. The way how the reconfigurability will be done is not part of this work although some research has been conducted on it and the Micro-Electro-Mechanical Switches (MEMS) are a promising technology for this kind of applications.

Chapter 3

Technical discussion

3.1 Receiving antenna diversity concept

In wireless communications, the multiple propagation paths of the mobile signal to the radio base-station antenna, or vice versa, results in short-term or fast-fading of the signal. This multiple path propagation channel often referred to as a Rayleigh fading channel experiences large drops in the received signal strength. These fading outages can be as large as 20-30 dB and occur rapidly over time as the mobile velocity increases.

Figure 3.1 summarizes the impairments of the wireless channel. As already known, one technique to mitigate these short-term fades is called receiving antenna diversity [7], in which the signals received over different antenna/channels are combined properly to increase the probability that the received signal is of adequate strength. The basic principle of antenna diversity is that multiple antenna outputs experience different signals due to different channel conditions, and these signals are only partially correlated. Thus, it is highly likely that if one antenna is in a deep fade, then the other one is not and provides sufficient signal, because in multipath propagation conditions, as encountered with a blocked or shadowed direct line-of-sight (LOS) path,

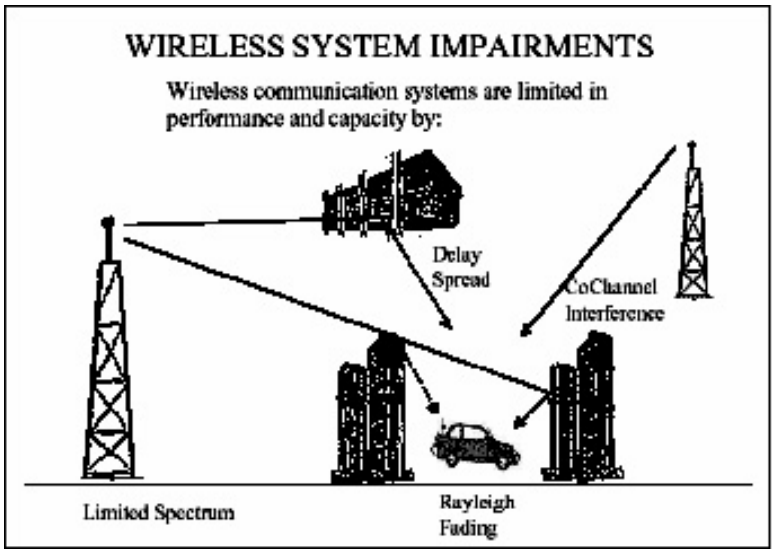

Figure 3.1: Impairments of the wireless channel.

each receive antenna experiences a different fading environment.

Depending on the severity of the fading, a fade margin often is necessary in the mobile link requirements to maintain a high degree of reliability in the communications link. Without this fade margin, the radio link is susceptible to increased noise in analog frequency modulated (FM) cellular systems and higher bit error rates (BER) for digital personal communication systems (PCS). In either case, reliable voice quality degrades, posing a serious concern for the mobile service provider.

Diversity antennas provide three major benefits:

1. Reliability is improved in multipath channels, where interference from reflected signals causes fading of the received signal. The fade level experienced on average for a given outage probability (percent down time) is decreased through diversity.

2. The overall average received signal power is increased. These signal increases can be dramatic.

3. It allow us to use lower transmit power for a given level or reliability. This

decreases interference, increases battery life of handheld radios, and reduces the probability that a hostile party will intercept the signals.

In fact, receiving diversity can be classified as a Single Input and Multiple Output (SIMO) communication scheme, that has as objective, to mitigate the multipath effect by trying to access to the maximum number of independent channels offered, at the receiver. Typically, antenna diversity is used only at the base station due to larger space available for the antenna system than in the mobile terminal, and hence, only the up-link fade margin is improved. However, with antenna miniaturization techniques and re-configurable capabilities, receiving diversity could start being employed at the mobile station too.

3.1.1 Classification of the diversity techniques

Receiving diversity techniques can be classified into five major types but many of them can be combined together for higher performance:

1. Space diversity.
2. Polarization diversity.
3. Pattern diversity.
4. Frequency diversity.
5. Time diversity.

Frequency and time diversity were not considered on this project because frequency diversity is difficult to use due to spectrum restrictions and system bandwidth requirements, and time diversity is based on redundant coding techniques, not electromagnetic aspects. Hence, the antenna diversity dimensions that have been investigated are: spatial separation, polarization and radiation pattern. The goal of any diversity scheme is to obtain uncorrelated signals. This decorrelation can be obtained

by locating the antennas at a distance large enough in space (spatial diversity), using distinct polarizations (polarization diversity) or beam patterns (pattern diversity).

3.1.2 Description of the diversity parameters

On this section we will introduce some of the parameters that are commonly used to evaluate the performance of diversity techniques. For this reason, we will limit ourselves to the particular case of two antennas, but the same parameters can be adapted to schemes with larger number of antennas.

Let us assume that $x_1(t)$ and $x_2(t)$ are the received signal voltages from a two antennas diversity scheme. Those signals, at the receiver, are passed to a combining or processing system to reduce channel distortion such as fading and co-channel interference, creating a signal $x_c(t)$. The amount of reduction in signal fading, or diversity gain, on $x_c(t)$, depends on two properties: the cross correlation and the relative signal strength levels between the received signals $x_1(t)$ and $x_2(t)$.

The average received signal strength at each of the antenna branches can be expressed as follows:

$$P_1 = E(|x_1(t)|^2) \tag{3.1}$$

$$P_2 = E(|x_2(t)|^2) \tag{3.2}$$

where E is the expectation. We can also define the complex cross correlation between the signals as follow:

$$\rho_c = \frac{E[(x_1(t) - \overline{x_1})(x_2(t) - \overline{x_2})]}{\sqrt{E[|x_1(t) - \overline{x_1}|^2]E[|x_2(t) - \overline{x_2}|^2]}} \tag{3.3}$$

where * is the complex conjugate and the bar indicates time average. It is also interesting to relate the envelope cross-correlation ρ_e between the signals with the

complex cross correlation:

$$\rho_e = |\rho_c|^2 \tag{3.4}$$

by assuming that the received signals have a Rayleigh-distributed envelope and randomly distributed phase. Under those definitions, typically, good diversity gain is said to be possible when the received signals satisfy the following two conditions, power imbalance and low correlation:

$$\rho_e < 0.5 \tag{3.5}$$

$$P_1 \approx P_2 \tag{3.6}$$

We can also obtain a close form expression for the envelope correlation as a function of the power correlation ρ_Γ for the correlated Rayleigh channel:

$$\rho_e = |\rho_c|^2 = \frac{(1-\sqrt{\rho_\Gamma})E(\frac{2\rho_\Gamma^{\frac{1}{4}}}{1+\sqrt{\rho_\Gamma}}) - \frac{\pi}{2}}{2-\frac{\pi}{2}} \tag{3.7}$$

where E() is the complete elliptical integral of the second kind (under the definition of the Jacoby elliptical integral with modulus k_2).

These parameters can be calculated directly by measuring the received antenna signals in a typical wireless environment. However, under certain assumption, those parameters can also be obtained from the radiation patterns and mutual coupling between antenna ports. In this way, the radiation pattern can be used to evaluated the cross-correlation as follows:

$$\rho_c = \frac{\int_0^{2\pi} A_{12}(\phi)d\phi}{[\int_0^{2\pi} A_{11}(\phi)d\phi \int_0^{2\pi} A_{22}(\phi)d\phi]^{\frac{1}{2}}} \tag{3.8}$$

where:

$$A_{nm}(\phi) = \Gamma E_{\theta m}(\frac{\pi}{2}, \phi) E^*_{\theta m}(\frac{\pi}{2}, \phi) + E_{\phi m}(\frac{\pi}{2}, \phi) E^*_{\phi m}(\frac{\pi}{2}, \phi) \tag{3.9}$$

in which:

$$E(\theta, \phi) = E_{\theta m}(\theta, \phi)\widehat{\theta} + E_{\phi m}(\frac{\pi}{2}, \phi)\widehat{\phi} \tag{3.10}$$

is the electric field pattern of each antenna and Γ is the cross-polarization discrimination (XPD) of the incident field. Again, last derivation is predicated on the fading envelope being Rayleigh distributed, the incoming field arriving in the horizontal plane only, the incoming field's orthogonal polarizations being uncorrelated, the individual polarization being spatially uncorrelated, and finally that the time-average power density per steradian is constant.

Estimates of the relative signal strengths can also be obtained from the antenna pattern using the mean effective gain (MEG). MEG is defined as the ratio of power received by the antenna along some random route to the total mean power incident to the antenna along the same route. Under the same assumptions as the ones stated on the previous paragraph, the MEG can be written as:

$$MEG = \int_0^{2\pi} [\frac{\Gamma}{1+\Gamma} E_\theta(\frac{\pi}{2}, \phi) + \frac{1}{1+\Gamma} E_\phi(\frac{\pi}{2}, \phi)] d\phi \tag{3.11}$$

If the antennas are 100% efficient then the maximum MEG is -3 dB, however, since this expression includes the antenna efficiency, then it's always lower than -3 dB.

The correlation between the antenna ports can also be obtained from the mutual coupling using the normalized resistance $r_{ij} = \frac{Re(Z_{ij})}{Re(Z_{ii})}$, using the expression that follows, where Z_{ij} are the standard two port impedances:

$$\rho_c \cong r_{ij} \tag{3.12}$$

This expression provides a quick method to measure cross correlation from the antenna terminal characteristics alone.

Finally, we used the diversity gain to quantify the improvement in signal to noise ration (SNR) of a received signal that is obtained using signals from different receiver branches. Diversity gain permits a direct comparison of improvement offered by multiple antenna sensors compared to a single one. The diversity gain for a given cumulative probability p is given by:

$$G_{div} = \gamma_{div}(p) - \gamma_1(p) \tag{3.13}$$

where $\gamma_{div}(p)$ is the SNR with diversity and $\gamma_1(p)$ is the SNR of a single branch without diversity combining. Diversity gain is the increase in SNR, due to diversity combining, for a given level of cumulative probability or reliability. Diversity gain is a function of branch correlation and power imbalance and decreases as the values of those two parameters increase.

3.1.3 Diversity processing techniques

The output signals from diversity antennas can be selected or combined in several ways to optimize the received signal power or Signal-to-Noise Ratio (SNR). Those are the main processing methods of combining the signal coming from the different antenna branches:

1. Selection Diversity (SD).
2. Equal Gain (EG).
3. Maximal Ratio Combining (MRC).

In selection diversity, the signal with higher SNR is selected, whereas in MRC, the signal from all the branches are weighted by their respective SNR, co-phased, and

added. EG employs the same algorithm as MRC but in that case the received signals are not weighted. Selection diversity is the less complex technique to implement but normally provides the lower diversity gain. On the other hand, EG and MRC are the methods that provides higher gains but at the expenses of more computing complexity and receiver architecture.

3.2 Reconfigurable antenna parameters for adaptive MIMO communications

Those are the parameters that have been considered as the possible ones to reconfigure in future adaptive Multiple-Input Multiple-Output (MIMO) [5] systems, and hence have been investigated from the antenna diversity gain perspective, on this project:

1. Distance between antennas: $d = 0.5\lambda$ and $d = 0.35\lambda$ in our case. At $d = 0.5\lambda$ the mutual coupling is approximately negligible while at $d = 0.35\lambda$ the mutual coupling for the ARSA is high, that is, the isolation between adjacent antennas is below 15 dB.

2. Type of polarization: linearly polarized and circularly polarized antennas.

3. Scheme orientation: the antenna diversity, using linear arrays, can be in the vertical ($\theta = 0°$) or horizontal direction ($\theta = 90°$). In figure 3.2 it is shown an schematic of an array in its horizontal and vertical orientation. The signal is assumed to arrive within small elevation angles from the XZ plane.

4. Type of antenna diversity: spatial, polarization and pattern diversity.

In the next sections we will present the MEA configurations that were used to investigate the influence of such parameters in the diversity gain with indoor fading MIMO environments.

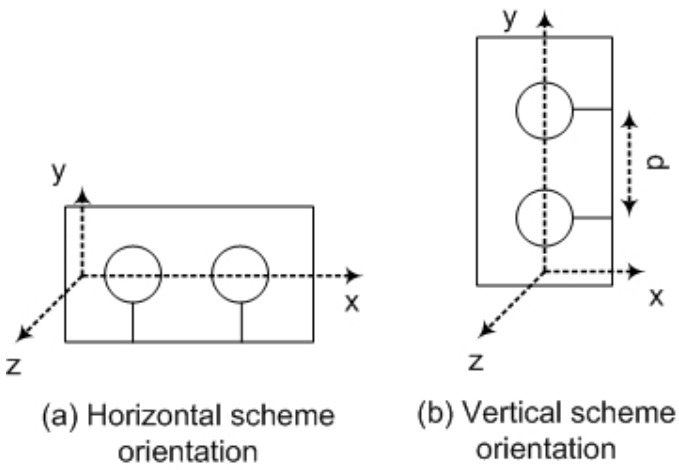

Figure 3.2: Schematics of an array of antennas in the (a) horizontal and (b) vertical orientation, when the signal is assumed to arrive within small elevation angles from the XZ plane.

3.3 Channel characterization and modeling

The first step to investigate the performance of the several receiving diversity techniques and schemes was to model the channel and identify the type of distribution that the signal presents at the receiver. The modeling technique was developed in a previous research work but on the following lines we present the procedure. The model that was used to describe the time response of the base-band wireless channel is given by the following equation:

$$c(t, x, y) = \frac{1}{d^{\frac{\beta}{2}}} \sum \alpha_k(x, y)\delta(t - k\tau) \tag{3.14}$$

where d is the distance between transmitter and the observation point (x,y), $\alpha_k(x, y)$ are the complex coefficients of individual multipath components and τ is the time resolution used in the model. The large-scale path loss exponent β is determined by a linear fit on the logarithmic of the average power channel profile for several points, inside the testing area. These profiles are normally obtained through measurements. Once these values are computed then the root-mean-square (rms) delay spread of the channel can be calculated, through the equation:

$$\tau_{rms}(t,x,y) = \frac{\sum_k (k\tau - \tau_m(x,y))^2 |\alpha_k(x,y)|^2}{\sum_k |\alpha_k(x,y)|^2} \tag{3.15}$$

where it was assumed that the first multipath component arrives at time zero and $\tau_m(x,y)$ is the mean excess delay defined as:

The quantity $\tau_{rms}(x,y)$ gives us an idea of the average delay in time at which the different replicas of the original signal, due to the multipath phenomena, arrive at the receiver.

Lognormal distributions are used for the fitting of experimental data. Because of the small expected $\tau_{rms}(x,y)$, the channel was modeled with single complex tap at frequency of interest, $f_0 = 2.45$ GHz, by simply taking the Fourier transform of the following equation:

$$C(f_0,x,y) = \sum_k \alpha_k(x,y) e^{-\imath 2k\pi f_0 \tau} \tag{3.16}$$

where the large-scale path loss contribution was removed. Doing that, it was possible to obtain the magnitude of $C(f_0,x,y)$ as well as the complex autocorrelation coefficient, calculated by the equation:

$$\rho_c(\Delta x, \Delta y) = \frac{E[C(f_0,x,y)C^*(f_0,x+\Delta x, y+\Delta y)]}{\sqrt{E[|C(f_0,x,y)|^2]}} \tag{3.17}$$

Rayleigh and Nagakami distributions were used to fit the distribution of $|C(f_0,x,y)|$. Note that the Nagakami distribution for the channel envelope is given by the equation:

$$f(r) = \frac{2m^m r^{2m-1}}{\Gamma(m)\Omega^m} e^{-\frac{mr^2}{\Omega}} \tag{3.18}$$

where $\Omega = E(r^2)$ and $m = \frac{\Omega^2}{Var(r^2)}$. Also note that there is a relation between the Nagakami and the Rice distribution through the parameter m above and the Rice factor K, which is the ratio of the power of the line of sight (LOS) component to that of the multipath:

$$m = \frac{(k+1)^2}{2k+1} \tag{3.19}$$

Different channel models other than the ones given in the baseband wireless channel equation are considered when slow channel variations (slow fading) must be separated from fast fading characteristics. This separation between slow and fast fading is important in the antenna diversity prediction, since the former one (slow fading) does not affect diversity. The procedure followed to compute the diversity gain is described later on this thesis.

The existence of multiple environments such as: rural, urban, suburban, indoor, outdoor; all of them with different propagation characteristics, allows us to classify the channels into those main sets: scattered and non-scattered channels, with Line-Of-Sight (LOS) and No-Line-Of-Sight (NLOS) channels. It is known that the wireless channels are a combination of those sets in all its possible grades. However, a Rayleigh model applies better for NLOS scattered environments, while a Ricean model work better for scattered LOS channel characteristics. Because on this project we are interested in employing receiving diversity techniques to improve communications on scattered environments, those were the two main models to consider. In indoor communications, were this project focuses on, Rayleigh distribution approximates the best the channel because most of the times, the indoor channel is a highly scattered NLOS channel.

Even the channel can be modeled as explained above, even more accurate simulation tools of a true realistic MIMO channel are complex and difficult to contrast with a real environment, arising the necessity for an experimental work to trully characterize the channel and scheme characteristics. Common assuptions of the incomming multipath field model are:

- The fading signal envelope is Rayleigh distributed.
- Orthogonals polarization are uncorrelated.
- The incomming field only arrives in the horizontal ($\theta = \frac{\pi}{2}$) plane.

Simulations of a true realistic MIMO channel are complex and difficult to contrast with a real environment, arising the necessity for an experimental work to trully characterize the channel and scheme characteristics without any assumption. Additionally, common not assumed issues in such models are:

- Cross-polarization coupling: which accounts for oblique reflections from walls and scattering from indoor clutter that produces coupling between orthogonal polarizations.
- Different path losses among different polarizations: which accounts for different transmission coefficients through the walls (Brewter angle).
- Different CDF of the signal (SNR at a given probability) among different polarizations.

3.4 Description of the radiating element

On this section we will describe the type of radiating element used in all the diversity schemes. The same radiating antenna element was used in all the diversity schemes and in all the techniques. We decided to employ as a radiating element a microstrip-feed coupled annular ring slot antenna. The main reasons are its large bandwidth, in terms of Voltage Standing Waver Ratio (VSWR) and Axial Ratio (AR), and compactness.

3.4.1 Annular ring slot antenna (ARSA)

The annular ring slot antenna is a broadband antenna very suitable for the incoming wireless communication applications. This antenna is planar and could be fabricated on the outer surface of a mobile unit. The antenna is easily excited by a microstrip feedline on the backside of the antenna. The metallization of the ARSA serves as the ground plane for the microstrip lines. Although those results are not included on this

study, this antenna is also suitable for coplanar-waveguide (CPW) feed mechanisms, while preserving the same broadband and compactness properties. This antenna, when excited on its fundamental mode, provides an omnidirectional radiation pattern.

The slot-ring antenna is one class of radiating structures formed from a ring gap or hole in an otherwise continuous metallic sheet. The sheet may or may not be backed on one side by a dielectric layer. In our case, it was backed. Both the conducting sheet and the dielectric are assumed to have some loss. The slot-ring structure is the mechanical dual of the microstrip-ring resonator. Figure 3.3 shows the ARSA (b-d) and its dual microstrip resonator (a-c).

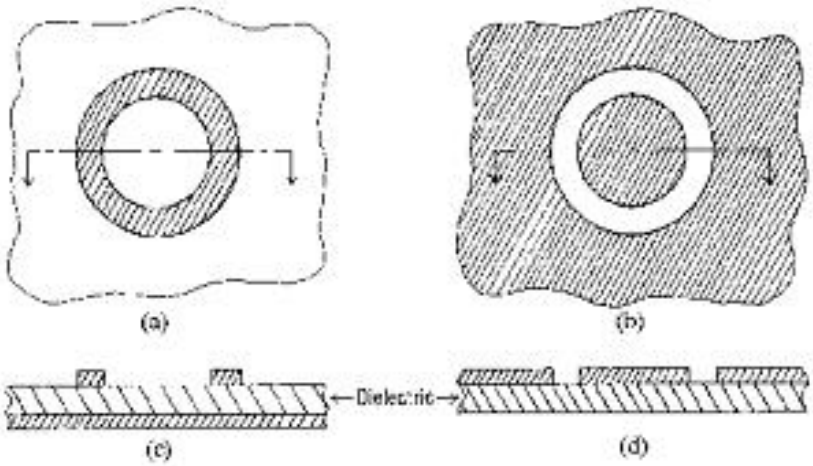

Figure 3.3: Top view and side view or the ARSA (b-d) and its dual microstrip resonator (a-c).

For analysis purposes, the ARSA antenna can be considered a segment of slot line bent into a loop. Like the microstrip resonator, the slot-ring structure's resonant modes occur at frequencies for which the ring circumference equals an integral number of guide wavelengths. To use the structure as an omnidirectional antenna, the first-order mode is excited as shown in figure 3.4.

Neglecting the other modes, the impedance seen by the voltage source (see figure 3.4) will be real at resonance, and all the power delivered would be radiated. The main questions regarding the design of this antenna to operate at a certain frequency

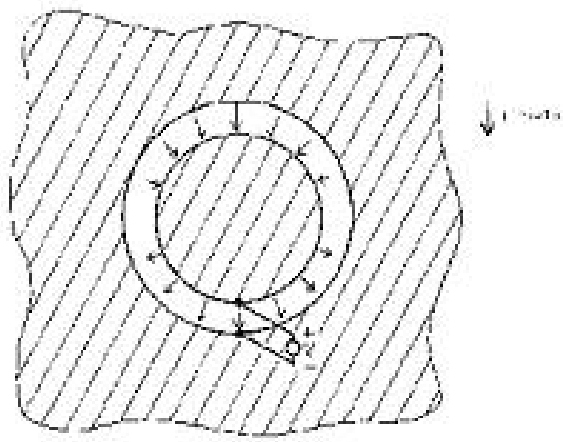

Figure 3.4: Distribution of the electric field on the slot, in the first-order mode of excitation, in the ARSA.

are how to compute the resonant frequency of the structure, how to determine its radiation pattern and how to find the input resistance at resonance.

The annular slot antenna, in its single feed configuration, can be seen as an open-ended coaxial line mounted on an infinite ground plane. Levine and Papas [9] derived that the width of the slot should not exceed the first root of the following equation:

$$J_0(ka)N_0(kar) - J_0(kar)N_0(ka) = 0 \tag{3.20}$$

where $R = \frac{2\pi}{\lambda}$ and $r = \frac{b}{a}$, that is, the ratio of the outer and the inner radii of the coaxial line. In order to provide an omnidirectional radiation pattern, it is necessary to maintain a constant electric field in the slot. Using a narrow slot fulfills this condition, and that happens when the slot with is much smaller compared to free space wavelength λ_0 at resonant frequency.

As described on [10], in the following lines we will present the design parameters of the annular ring slot antenna. The slot radius is derived from the dependence of the filed patterns on free space wave number $k_0 = \frac{2\pi}{\lambda_0}$. It is found that if the product of the radius, a, and k_0 is equal to 1 or 2, then the omnidirectional radiation pattern is obtained which is evident from the radiation patter equation showed below:

$$R(\theta) = \frac{W_s^2 k_o^2 E_o^2 a^2}{4\gamma^2} J_1^2(ak_1 \sin\theta) \tag{3.21}$$

which is equivalent to say that the slot length needs to be equal or the double of the wavelength in the slot.

In our case, a microstrip line at the bottom of the substrate feeds the annular ring slot antenna. The feed line crosses the slot and terminates in an open-circuit. For proper matching, the length of the line beyond the intersection with the slot is kept $\frac{\lambda_s}{4}$, with λ_s being the slot wavelength. The reason why the feed line is extended approximately a quarter wavelength beyond the slot has to do with the fact that since the line is open-ended, the line sees a shortcut at the intersection with the slot, allowing maximum coupling of the electric field into the slot and hence the maximum amount of energy can be radiated through the slot. The approximate value of λ_s is obtained from the following expression:

$$\lambda_s \approx \lambda_0 \sqrt{\frac{2}{(\epsilon_r + 1)}} \tag{3.22}$$

The previous expression gives a length slightly longer than the actual required value, so in general it requires some trimming for proper impedance matching. A more accurate expression for this length is provided on [13] by the following equation:

$$\lambda_s = \lambda_0[1.045 - 0.365 \ln \epsilon_r + \frac{6.3(\frac{w_s}{h})\epsilon_r^{0.945}}{238.64 + 100\frac{w_s}{h}} - [0.148 - \frac{8.81(\epsilon_r + 0.95)}{100\epsilon_r}] \ln(\frac{h}{\lambda_0})] \tag{3.23}$$

where w_s is the slot-line width and λ_0 is the free-space wavelength. The antenna input impedance is obtained from:

$$Z_a = R_a + jX_a = \frac{1}{\frac{1}{R} + jwC + \frac{1}{jwL}} \tag{3.24}$$

where $L = \frac{R}{2\pi f_r Q_T}$, $C = \frac{Q_T}{2\pi R f_r}$ and Q_T is the quality factor. The resistive part of the input impedance can be found from closed form approximation as:

$$R = 72.62 - 35.19\log\epsilon_r + 50\frac{(\frac{W}{h}-0.02)(\frac{W}{h}-0.1)}{\frac{W}{h}}$$
$$+\log(\frac{W}{h}100(44.28 - 19.58\log\epsilon_r))$$
$$-[0.32\log\epsilon_r - 0.11 + \frac{W}{h}(1.07\log\epsilon_r + 1.44)](11.4 - 6.07\log\epsilon_r - \frac{h}{\lambda_0}100)^2 \quad (3.25)$$

On the other hand, the quality factor, Q_T is obtained from the total energy stored, W_T and the radiated power, P_r, as follows:

$$Q_T = \frac{wW_T}{P_r} \quad (3.26)$$

Some other design parameters are the antenna directivity (D), gain (G) and radiation efficiency (η), which are obtained from the following equations, respectively:

$$D = \frac{5}{\int_0^\pi J_1^2(ak_0\sin\theta)d\theta} \quad (3.27)$$
$$\eta = \frac{P_r}{P_t} \quad (3.28)$$
$$G(dB) = 10\log(D\eta) \quad (3.29)$$

Finally, the antenna bandwidth is defined as the frequency range over which the Voltage Standing Wave Ratio (VSWR) increases from unity to a tolerance limit S and is expressed as:

$$BW = \frac{S-1}{Q_T\sqrt{S}} \quad (3.30)$$

We decided to use a slot antenna for its larger bandwidth with respect to its equivalent microstrip version, while preserving similar radiation patterns and efficiencies. In particular, the annular ring slot antenna is very compact in size and is then suitable for studying MEA schemes. Microstrip coupling feed was adopted for its higher bandwidth and simplicity with respect other feedings mechanism like aperture coupled or coplanar-waveguide (CPW).

3.4.2 Multi-port annular ring slot antenna (M-ARSA)

The annular ring slot antenna has also been studied when fed in multiple ports. It has been proven on [13] that for narrow slots, the magnetic current, M_ϕ, is constant across the slot. The magnetic current can be expanded in a Fourier transform series:

$$M_\phi(r,\phi) = f(r) \sum_{m=-\infty}^{\infty} c_m e^{\imath m\phi} \tag{3.31}$$

where $f(r)$ is 1 in the slot, and 0 elsewhere. The method described on [13] allows to determine the coefficients c_m and hence the magnetic current, from the feed current density and by applying the Hankel transformation and Galerkin‘s procedure. Then, for an annular slot antenna feed at multiple ports, the driving point self-impedance is therefore:

$$Z_{ii} = \frac{2Z_0}{\pi}(k_0 w)^2 \sum_{m=-\infty}^{\infty} \frac{1}{K_m} \tag{3.32}$$

where K_m is the normal susceptance of each of the azimuthally resonant modes. The mutual impedance can be derived by considering a pair of feeds. If we assume that the slot is excited by feed j at angle position $\phi = \phi_j$ and by feed k at $\phi = \phi_k$, then the mutual impedance can be expressed as follows:

$$M_\phi(r,\phi) = f(r) \sum_{m=-\infty}^{\infty} \frac{e^{\imath m(\phi_j - \phi_k)}}{K_m} \tag{3.33}$$

In particular, for a two-port annular slot antenna, an in-phase (sum feed) results in a driving point impedance of $Z_{11} + Z_{12}$, whereas an anti-phase feed (difference feed) yields a driving point impedance of $Z_{11} - Z_{12}$. In the case of a quadrature feed, each port sees different impedance $Z_{11} \pm \imath Z_{12}$.

On the other hand, shorted annular slots are used to increase the flexibility of the antenna without adding extra feed lines, in particular to provide circular polarization radiations. In the general case, if we assume that port n is shorted, then, the remaining

n-1 ports form an n-1 port-radiating network in which the mutual impedance can be written as follows:

$$Z'_{jk} = Z_{jk} - \frac{Z_{jn}Z_{nk}}{Z_{nn}} \tag{3.34}$$

The far-field radiation pattern can be again calculated from the Hankel transformed aperture field, which is the radiating magnetic current in the case of the annular slot antenna. In the general case for multiple feed ports, the far field can be obtained once the coefficients c_m are known for any feed arrangement.

3.4.3 Substrate considerations

The substrate used to simulate and fabricate the radiating antenna elements and the diversity schemes was RT/Duroid Roger 5695, with dielectric constant $\epsilon = 2.50$ and thickness h=1.1938 mm. Low dielectric constant substrate is appropriate for antenna applications because the radiation efficiency can be high. A thick substrate is also interesting because the achieved bandwidth is in general larger in thicker substrates, although it cannot be too thick neither in order to prevent the surface wave phenomena when combining those antennas in an array disposition, which could decrease the total radiation efficiency.

3.5 Different configuration of the radiating element

On this section we will describe four different configuration of the same radiating antenna element that have been designed and fabricated to be used in the different diversity techniques. The configurations are:

1. Linearly polarized ARSA.
2. Dual linearly polarized ARSA.

3. Circularly polarized ARSA.

4. Dual circularly polarized ARSA.

Those configurations hence, allow us to study each diversity technique and any combination of them: space, polarization and pattern diversity. The design and simulations of those antenna configurations were conducted with the software HFSS 8.0-9.0, based on the Finite Element Method (FEM) and/or ADS from Agilent based on the Method of Moments (MoM), and very close agreement with the measurements was observed.

3.5.1 Linearly polarized ARSA

The single feeding configuration in the annular slot ring antenna, without any perturbation in the slot, provides a radiating antenna element that is linearly polarized. On this configuration, the slot length is approximately one wavelength. However, the resonant frequency of this structure is very dependent on the feedline, in particular its offset from the intersection with the slot, that is, the distance l_m in figure 3.5. It has been notice that by reducing this offset, the resonant frequency decreases and then it provides a way to further reduce the size of the antenna. That is, by considering the slot length approximately one wavelength on the slot, we could compute its diameter as follows: $2\pi R = \lambda_g \Rightarrow R \approx 0.159\lambda_g \Rightarrow D \approx 0.318\lambda_g$. By reducing the length l_m, the diameter could be further reduced up to $D \approx 0.26\lambda_0$, which makes this antenna compact and very suitable for array configurations studies.

To operate at 2.45GHz the dimensions of the antenna were calculated to be the following: slot radius $r_s = 15.3$ mm, slot width $w_s = 2.2$ mm, $l_m = 5.8$ mm, and feedline width $w_m = 3.4$ mm to provide a 50Ω microstrip line on this substrate. In figure 3.5 it is shown the schematic of the antenna on this configuration and the axis definition that will be used to presents the simulation and measurement results. Figure 3.6 shows a picture of the fabricated antenna.

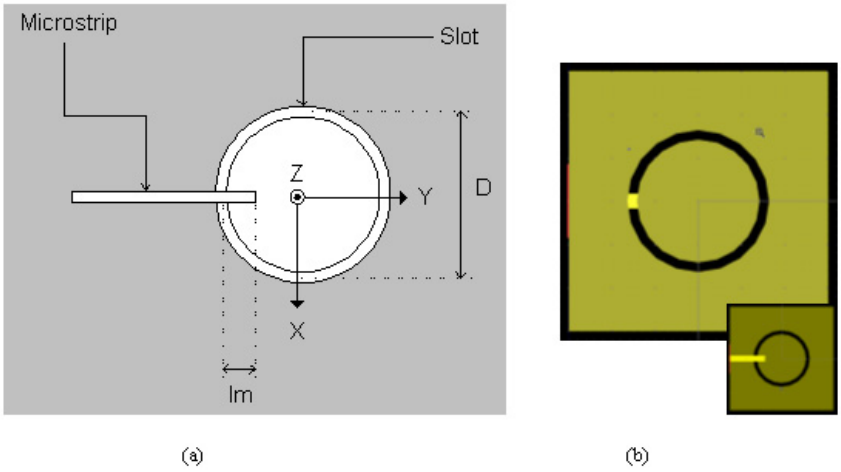

Figure 3.5: (a) Schematic of the linearly polarized ARSA and coordinate system orientation, (b) layout on HFSS software.

Under this configuration and coordinate system, the radiated electric field is linearly y polarized.

Simulations and measurements of the linearly polarized radiating element

In the next lines the simulations results corresponding to the linearly polarized configuration will be presented. Figure 3.7 shows the theoretical and measured return loss.

As we can observe, the resonant frequency is centered at 2.45GHz and the input impedance bandwidth, that is, the frequency range where the Voltage Standing Wave Ratio (VSWR) is equal or lower than 2, is approximately 11%. Figure 3.8 show the simulated and measured radiation pattern of the antenna on its main two cuts: XZ plane and YZ plane. The maximum gain of the antennas was around 4 dBi and the Half-Power-Beamwidth (HPBW) of 100°.

In all the cuts the co-cross polarization level, or isolation between the phi and theta components of the electric field, is larger than 15 dB and hence it is suitable for its use as a linearly polarized antenna. It provides an omnidirectional radiation pattern in the XZ plane which makes the antenna suitable for personal communications and

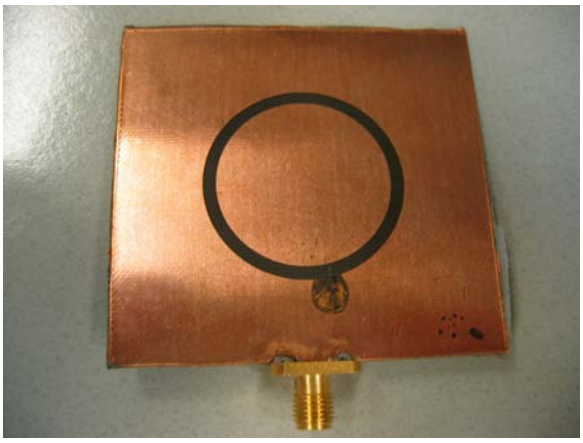

Figure 3.6: Fabricated linearly polarized ARSA.

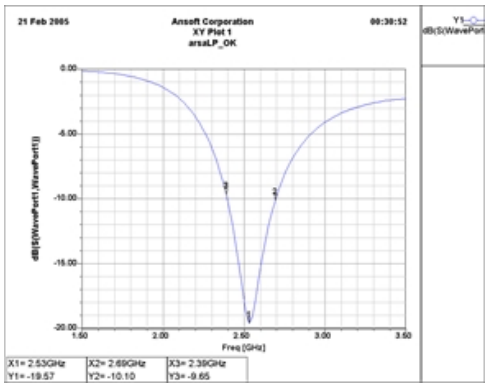

Figure 3.7: Simulated (solid line) and measured (dashed line) return loss.

mobile terminals. The measurements and the simulations are in close agreement, making the HFSS software a very useful design tool.

3.5.2 Dual linearly polarized M-ARSA

The annular slot ring antenna, when fed from two orthogonal locations on the slot (Multi-port ARSA), can be used to extract two orthogonal polarizations simultaneously. During the design, the slot radius needed to be slightly increased for two reasons: to compensate the multi-port feeding mechanism that shifted up the res-

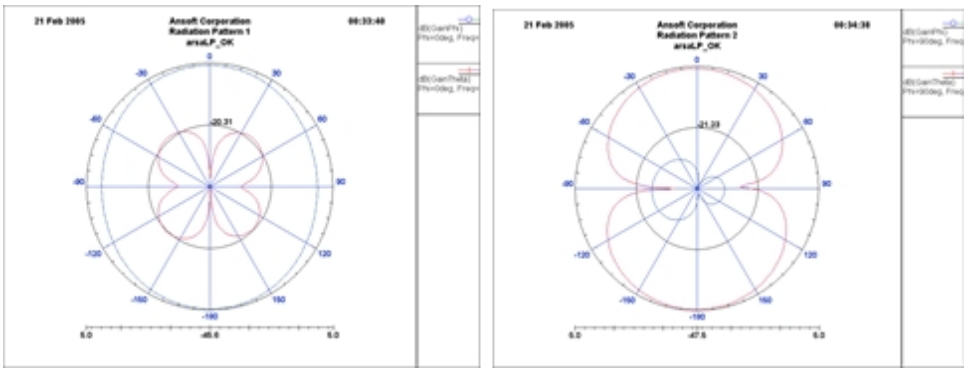

Figure 3.8: Simulated radiation pattern of the antenna on its main two cuts: XZ plane (left) and YZ plane (right)

onant frequency of the structure, and to shift intentionally the resonant frequency slightly away from 2.45GHz in order to increase the isolation between ports to an acceptable level of at least 15 dB. In figure 3.9 we show a schematic of the antenna on this configuration.

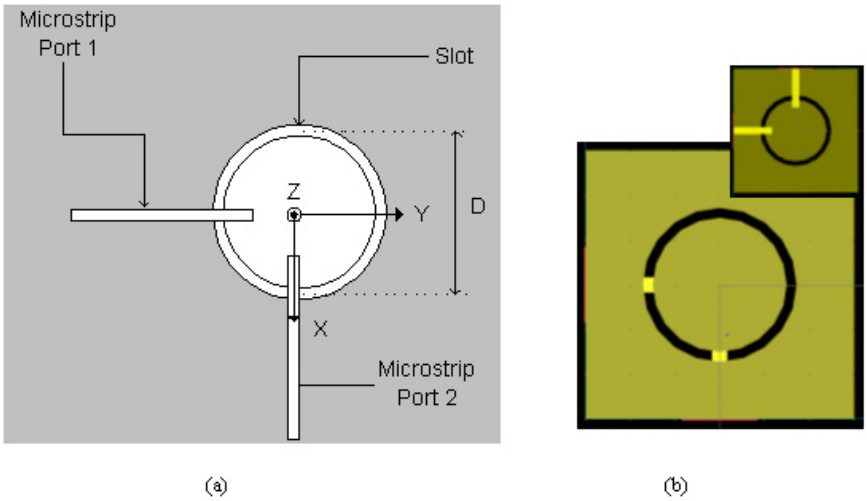

Figure 3.9: (a) Schematic of the dual linearly polarized ARSA and coordinate system and (b) layout on HFSS software.

The antenna dimensions on that case were: slot radius $r_s = 16.1$ mm, slot width $w_s = 2.2$ mm, feedline offset (AC distance) $l_{m1} = 4.9$ mm and $l_{m2} = 4.9$ mm, feedline width $w_m = 3.4$ mm, and port separation of 90°.

Simulations and measurements of the dual linearly polarized radiating element

Figure 3.10 shows the theoretical and measured return loss and isolation.

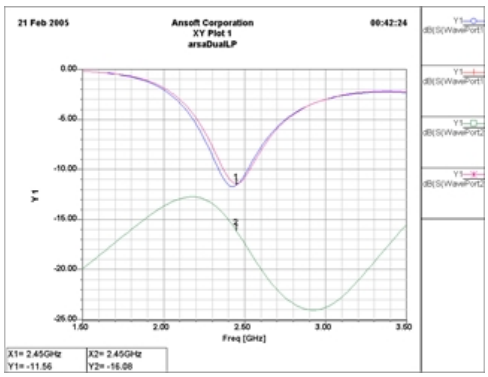

Figure 3.10: Simulated (solid line) and measured (dashed line) return loss.

The resonant frequency for both ports is centered at 2.40 GHz and the input impedance bandwidth is approximately 9%. The isolation between polarization ports at 2.45 GHz is around 16 dB. Figures in 3.11 show the simulated and measured radiation pattern of the antenna on its main two cuts for one of the ports: XZ plane and YZ plane. The maximum gain of the antennas was around 4 dBi and the Half-Power-Beamwidth (HPBW) of 90°.

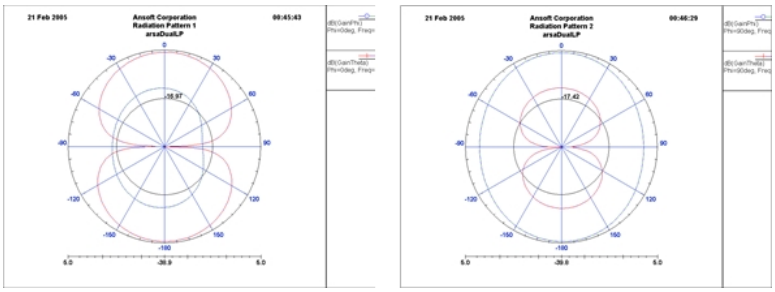

Figure 3.11: Simulated radiation pattern of the antenna on its main two cuts for one of the ports: XZ plane and YZ plane

In all the cuts the co-cross polarization level, or isolation between the phi (horizontal) and theta (vertical) components of the electric field, is larger than 15 dB

and hence each port can be seen as an independent linearly polarized antenna. The radiation patterns for the other port are almost the same in shape, with the only difference that the electric field components need to be exchanged. It provides an omnidirectional dual polarized radiation pattern in the XZ plane which makes the antenna suitable for personal communications and mobile terminals.

Figure 3.12 shows a picture of the fabricated antenna.

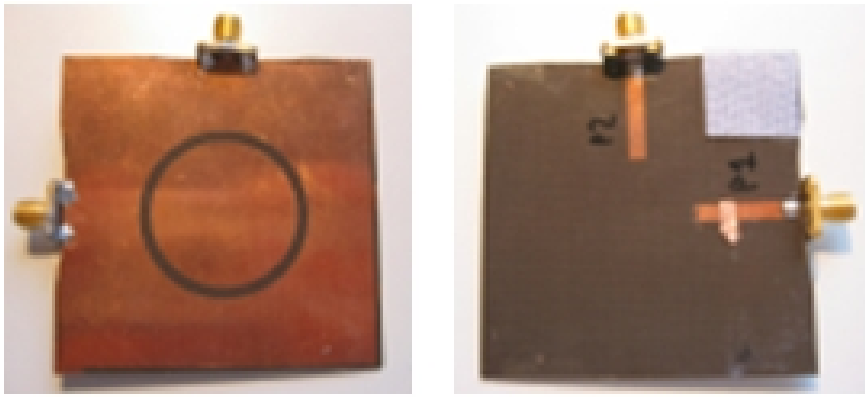

Figure 3.12: Fabricated dual linearly polarized ARSA.

3.5.3 Circularly polarized ARSA

The technique that has been used to get circular polarization radiation from the annular slot ring antenna is by shorting the slot at a particular point. There exist some other techniques to provide circular polarization to the antenna, like using two orthogonal feedings or by bending the slot at a point orthogonal to the feeding input point. The reason why the shorting technique was chose is because is the simplest one although the other techniques may offer some other advantages in terms of better bandwidth. In figure 3.13 we show a schematic of the antenna on this configuration.

The antenna dimensions on that case were: slot radius $r_s = 18.277$ mm, slot width $w_s = 2.2$ mm, feedline offset (AC distance) $l_m = 9.9$ mm, feedline width $w_m = 3.4$ mm, shorting location at $\phi = -71°$, and shorting width $w_{sc} = 0.2$ mm. As stated in

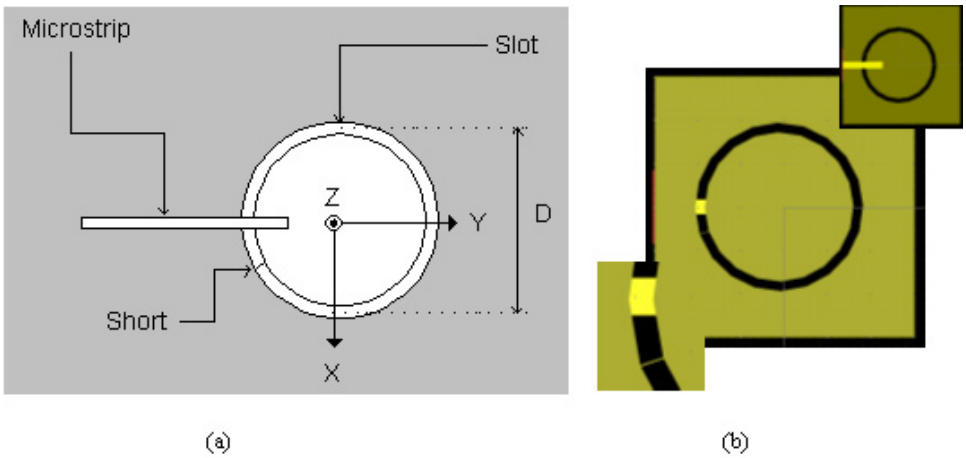

Figure 3.13: (a) Schematic of the circularly polarized ARSA and coordinate system and (b) layout on HFSS software.

the literature, for achieving circular polarization (CP) behavior by introducing some short on the slot, the slot length needs to be approximately 1.5 wavelengths on the slot. In our case, it was slightly smaller because we play with the feedline offset to reduce its dimension. Finally, figure 3.14 shows a picture of the fabricated antenna.

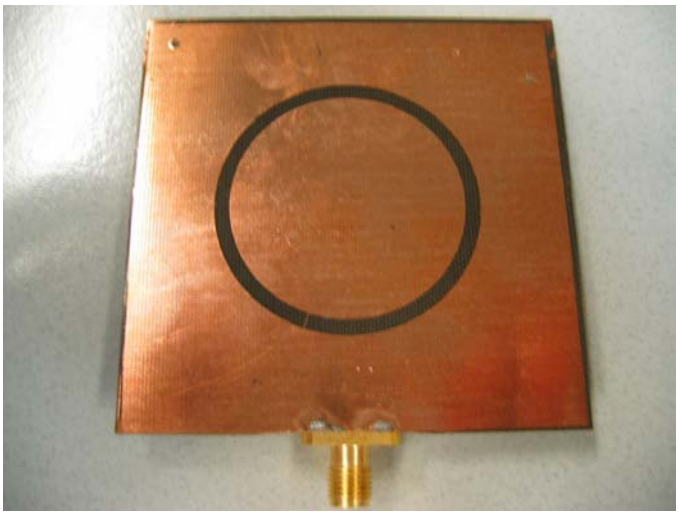

Figure 3.14: Fabricated circularly polarized ARSA.

Simulations and measurements of the dual circulary polarized radiating element

Figure 3.15 shows the theoretical and measured return loss.

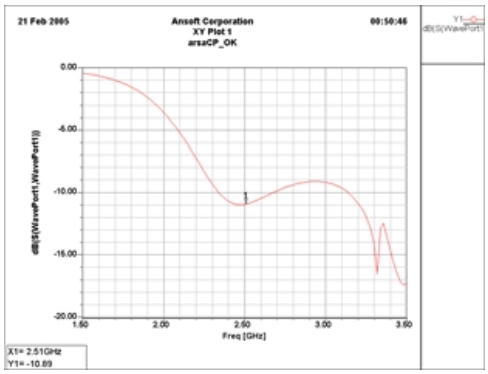

Figure 3.15: Simulated (solid line) and measured (dashed line) return loss.

The resonant frequency is centered at 2.45GHz and the input impedance bandwidth is approximately 12.6%. The axial ratio bandwidth is around 7%. Figures 3.16 show the simulated and measured radiation pattern of the antenna on its two main cuts: XZ plane and YZ plane. The maximum gain of the antennas was around 4 dBi and the Half-Power-Beamwidth (HPBW) of 90°.

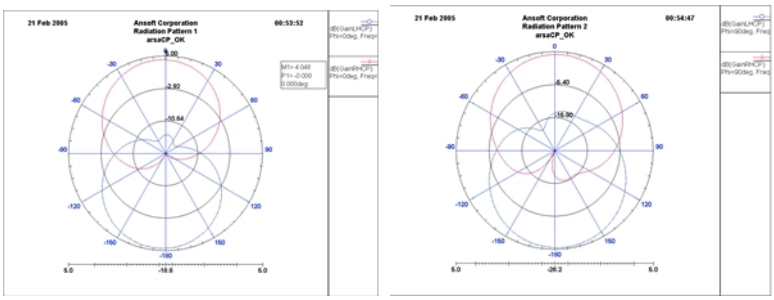

Figure 3.16: Simulated (solid line) and measured (dashed line) radiation pattern of the antenna on its main two cuts: XZ plane and YZ plane.

In all the cuts the co-cross polarization level, or isolation between the Right-Hand Circular Polarization (RHCP) and the Left-Hand Circular Polarization (LHCP) components of the electric field, is larger than 15 dB and hence suitable for its use

as a circularly polarized antenna. It provides an omnidirectional radiation pattern in the XZ plane, which makes the antenna suitable for personal communications and mobile terminals. By placing the shorting point on the right or the left side of the feedline, the antenna can radiate LHCP or RHCP respectively (on the $\theta = 0°$ propagation direction). In the opposite direction, $\theta = 180°$, the antenna is radiating in the opposite polarization.

3.5.4 Dual circularly polarized M-ARSA

This configuration is under study currently and it should allow us to extract the RHCP and the LHCP at the same time from the antenna. The idea is to use two shorting points and two orthogonal feeding points to be able to extract RHCP and LHCP individually. Some good initial results have been obtained but further investigation would need to be done to improve isolation between components.

3.6 Description of the non-radiating elements

On this section we will describe some other non-radiating elements that were also used on different diversity schemes. The T-juntion power divider and the 90° quadrature hybrid are the two non-radiating element and they were employed on pattern diversity schemes to combine or divide the RF power coming/going from/to the antennas.

3.6.1 T-junction power divider

The first type of power divider used on this study was a Wilkinson power divider based on the research work conducted on [8]. This component is used for power division and/or combination in many wireless communications systems. It is a miniaturized Wilkinson power divider by folding the quarter-wavelength section of the conventional topology into the meander-coupled line. As stated on previous research, it is

physically smaller and provides better electrical performance than the conventional one. The center frequency of this divider is determined by controlling the coupling distance and the electrical performance of the divider could be further improved by inserting slits. Figure 3.17 shows a schematic of the power divider with the main design parameters.

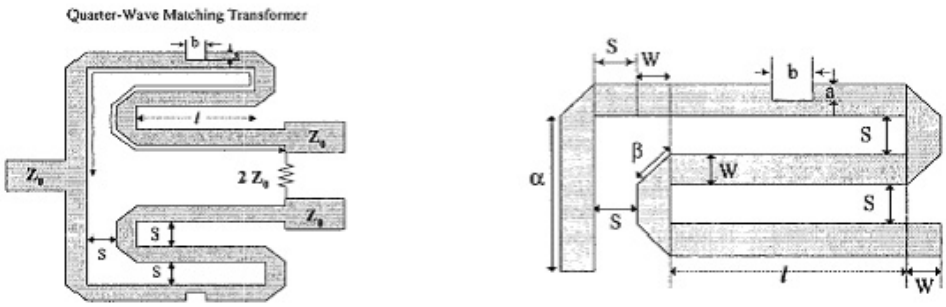

Figure 3.17: Miniaturized Wilkinson power divider.

The design parameters are related by the following equations:

$$\alpha + 3S + 3l + 2\beta + 2W = \frac{\lambda_g}{4} \tag{3.35}$$

where β is the length of bend, W is the width of microstrip, l is the length of commensurate line, and α is the required line for coupled structure which is determined to be approximately $\frac{\lambda_g}{16}$, where λ_g is the wavelength in the microstrip waveguide. An expression for the normalized coupling distance for the optimum operation is given by:

$$\frac{S}{\lambda_g} = 0.0153 \pm 0.001 \tag{3.36}$$

In our design, no slits were used to optimize the performance so we are not showing the design equations for them. After applying the previous equations, an optimization on ADS was performed to get the final design. A surface mounted 100Ω resistor, RR0510 (0402), from Susumu Co., was used to improve the isolation between ports.

This high frequency resistor was chosen for its good RF characteristics at 2.45GHz. In figure 3.18 we show its layout on ADS and a picture of the fabricated power divider.

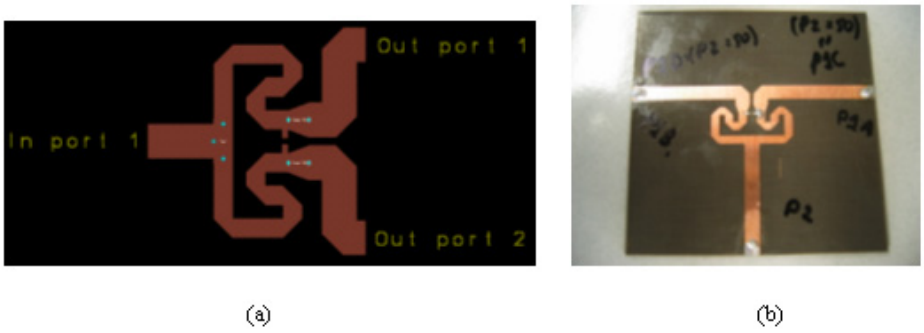

Figure 3.18: (a) Layout on ADS and (b) picture of the fabricated power divider to operate at 2.45GHz.

The main reason for using such a compact power divider over the conventional one, is for compactness, because the space in pattern diversity schemes is very limited and in particular for planar arrays configurations.

Simulations and measurements of the T-junction power divider

In the first figure (left) of 3.19 it is showed the simulated and measured return loss for each one of the three ports. The second figure (center) in 3.19 shows the isolation between ports and the third (right) one shows the approximately -3 dB insertion loss between the input and the two output ports.

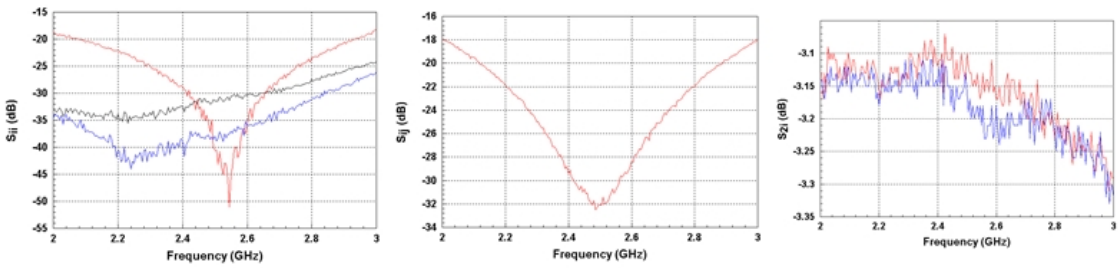

Figure 3.19: Simulated and measured return loss, insertion loss, and isolation.

3.6.2 90° hybrid power divider (Butler Matrix)

The second type of power divider used on this study was a 90° quadrature hybrid. This component was also used to divide and/or combine the power. The 90° quadrature hybrid is in fact a Butler matrix [11][1][2][4] for 2 elements. The Butler matrix was used to investigate the performance of the pattern diversity. The center frequency of the hybrid was at 2.45 GHz. Figure 3.20 shows a picture of fabricated component.

Figure 3.20: Fabricated 90° hybrid power divider

Simulations and measurements of the 90° hybrid power divider

The measurements showed an approximately value of -3 dB insertion loss between the input and the two output ports. The return loss of the ports below -20 dB and a phase delay between the isolated output port of approximately ±90°. The sign of the phase depends on which of the input ports is exited.

3.7 Multi-Element-Antenna (MEA) configurations

On this section we will describe the receiving diversity techniques and schemes that have been investigated. In addition, some simulation and measurement results will be presented regarding mutual coupling, the return loss, the isolation and the radiation patterns characteristics. At this point, no results concerning the receiving diversity gain are included, those will be presented later on this thesis. The simulation tool to evaluate the electrical performance of the diversity schemes was ADS from Agilent. This software is base in the Method of Moments, and provides faster simulation at array level design than HFSS 8.0. This work focuses on linear arrays only, leaving the planar configurations for future work.

Two are the main parameters we have focused on this work concerning the electrical characteristics of the linear arrays:

1. Mutual coupling due to field interaction between adjacent antennas: affects the correlation of the signal.
2. Radiation pattern deformation: due to mutual coupling and that affects the correlation and the power imbalance of the signal.

On this project we have considered 10 antenna diversity schemes based on the 2x1 antenna annular ring slot antenna array. From those schemes, 6 of them were used to investigate spatial and pattern antenna diversity, while 4 of them were used to investigate polarization diversity. They are described in the following sections.

3.7.1 MEA schemes to investigate spatial and pattern antenna diversity

A rule of thumb for spatial diversity in mobile communications follows as a half-wavelength separation between omnidirectional antennas, although much closer spacing is possible if the environment is enough dispersive and the angular spread is

large enough. In space diversity, correlation coefficients lower than 0.5 are considered low enough to provide good diversity gain. Typical antenna separations are equal or larger than 0.5 wavelengths. Clarke derived the following relationship between envelope correlation ρ_e and antenna separation in [3]:

$$\rho_e \cong J_0^2(\frac{2\pi d}{\lambda}) \tag{3.37}$$

where J_o is the Bessel function of the first kind with order zero, d is the antenna spacing, and λ is the wavelength. This expression is valid for a uniform angle of arrival distribution in azimuth and identically polarized omnidirectional receiving antennas that are matched to the polarization of the incoming wave. All multipath components are assumed to lie in the horizontal plane. It needs to be said, that the correlation predicted by this formula is in general higher than in reality, especially for smaller separations. The reason is because this formula doesn't take into account the mutual coupling between the antenna elements at a given distance. In reality, it has been noticed that the correlation between the envelopes of signals received by two antennas is decreased if the patterns of each antenna are different. This is because the relative amplitudes and phases (weights) of the incident multipath signals are different at each antenna, even if the antennas are collocated. And the reason why the patterns of closely spaced antennas that are omnidirectional in free space are distorted is due to the mutual coupling. On the other hand, for distances enough large so that the mutual coupling can be considered negligible, it is true that the larger the separation the lower the correlation. This idea can be observed in figure 3.21.

Concerning pattern diversity, this technique creates multiple beams in different directions to access the uncorrelated signals. Pattern diversity, in fact, have inherent space diversity due to antenna separation necessary to create those beams.

In any case, in pattern diversity, antennas with narrow beam-width are positioned in different angular directions or regions. The two main reasons narrower beams are used are to increase the gain of the base-station antenna and to provide angular discrimination that can reduce interference. Two are the techniques to achieve narrow

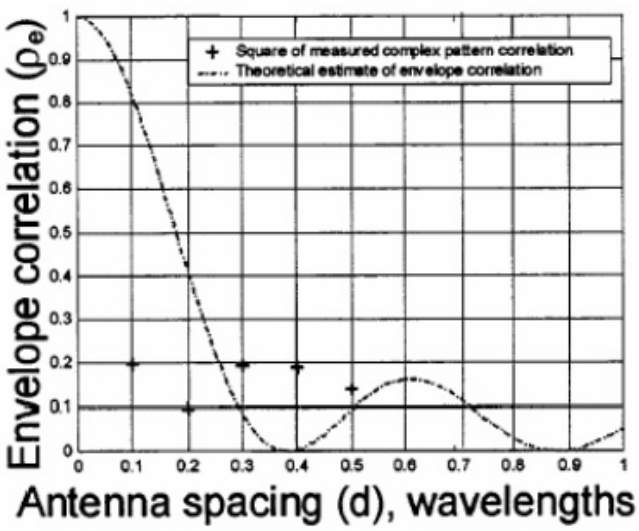

Figure 3.21: Theoretical (line) and experimental (crosses) envelope correlation vs. antenna spacing.

beam-width: first by using directive antennas and secondly by using omnidirectional antennas in an array configuration, connected to an external network, such as the Butler matrix in our case, to create directional beams. In both cases, there is a tradeoff between the narrow beam-width, or gain, and the number of antenna beams, and hence, the complexity and size of the antenna, which produces the multiple narrow beams.

In addition, in pattern diversity there are two possible approaches, the static approach and the dynamic approach. In the static approach, multiple beams are created and are always present so that later by applying some diversity combining techniques, some diversity gain is obtained. In the dynamic approach, one single beam is created but on this case is adaptive and dynamically changed to track the signal of interest. On this project we have focus on the static approach, first because it's implementation is simpler and doesn't need any tracking or adaptive control algorithm, and secondly because the static approach seems intuitively better for highly scattered environments where the angle of arrival of the main received signals can changes rapidly, so that it would be a really difficult task to keep track of an almost random signal like this one.

Mutual coupling has also a significant effect on the pattern diversity but there is not still clear answer regarding its effects on diversity gain. However it's know that the mutual coupling is going to affect the overall radiation pattern and this one will differ from the predicted one from array theory because that theory assumes that all the antenna elements have the same radiation pattern but in reality, due to mutual coupling that's no longer true. Actually from this point of view, we can have pure pattern diversity because all the beams share the same antennas and all of them are affected in the same way by the mutual coupling.

It's important to know that given a linear array of omnidirectional antenna patterns, the total radiated pattern is the product of the called array factor (AF) times the radiation pattern of each individual antenna, that is:

$$\overline{E}(\overline{r}) = \overline{E_0}(\overline{r})AF(\psi) \tag{3.38}$$

where $AF(\psi) = \Sigma_{n=0}^{N-1} a_n e^{\imath n\psi}$ and $\psi = kd\cos\theta + \alpha$. In the previous formulas, d is the separation between antennas, a is the progressive current phase between antennas, an is the magnitude of the current for antenna n, N is the total number of antennas, and k is the wave number in the media. This equation allows us to obtain the necessary configurations for the currents, number of antennas and separation, to create a desired beam in a certain desired direction.

In other words, pattern diversity is when the same pattern is spaced in angle, that is, rotated, rather than in distance. A rule of thumb for pattern diversity is that under the assumption of uniform scenario, where the angle spread is almost uniform in all directions, the 0.7-decorrelation angle is half of the half-power beam-width (HPBW) of the antenna. This handy result is independent of the pattern bandwidth, as long as the beam is well within the circular support. In practice, the side-lobe structure and non-uniform phase of a real-world pattern will make the de-correlation angle smaller, so the above rule-of thumb is interpreted as an upper limit for the minimum de-correlation angle for a uniform scenario. In fact the de-correlation angle spread depends on the spread of the beam and scenario uniformity. Under the assumption of

Gaussian beams, the power correlation coefficient in terms of beam separation angle can be expressed as follows:

$$\rho(\Omega) \approx e^{\frac{-\Omega^2}{2\sigma_p^2}} \tag{3.39}$$

where:

$$\sigma_\rho^2 = \sigma_g^2(\frac{\sigma_g^2}{\sigma_s^2} + 2) \tag{3.40}$$

and where σ_ρ^2 is the spread of the correlation coefficient, σ_g^2 is the spread of the beam and σ_s^2 the spread of the scenario. As a note, the power correlation coefficient can be related to the envelope correlation coefficient by $|\rho(\Omega)|^2 \approx \rho_e(\Omega)$. If we define the 0.7-decorrelation angle, Ω_d as the one that provides $\rho_e(\Omega_d) = 0.7$, and for a sufficient directive beams, that is, as long as the HPBW is less than about 90 (directivity less than 6 dB), then is found that:

$$\rho_e(\Omega_d) \approx e^{\frac{-\Omega^2}{2\sigma_p^2}} \Rightarrow \Omega_d \approx HPBW\sqrt{\frac{1}{8}\frac{\sigma_g^2}{\sigma_s^2} + \frac{1}{4}} \tag{3.41}$$

When $\frac{\sigma_g}{\sigma_s} \geq 3$, and in particular for the uniform scenario, then the 0.7-decorrelation angle is half of the half power beam-width of the antenna pattern as given by the following expression:

$$\Omega_d \approx \frac{HPBW}{2} \tag{3.42}$$

Finally it's interesting to notice that directive scenarios, like LOS or non-highly scattered environments, result in an increase of the de-correlation angle. The underlying idea behind pattern diversity is that in other to provide pattern diversity it is required to provide uncorrelated radiation patterns or beams.

The beams created by the Butler matrix have been shown in the literature to provide very low level of correlation in indoor environments. This is the reason for using a Butler matrix on this study.

Vertically linearly polarized scheme at $d = 0.5\lambda$ antenna separation (scheme 3.7.1.1)

This scheme is a 2x1 linear array of antennas separated $d = 0.5\lambda$ and vertically linearly polarized.

In this scheme the mutual coupling between antenna elements is small (isolation is approximately of 18 dB) and hence this scheme is used to investigate the performance of such diversity schemes with negligible mutual coupling, when the antennas have a linear polarization oriented in the vertical direction.

In particular, because the distance is 0.5λ the radiation patterns were not distorted and this scheme becomes very adequate to investigate pure spatial diversity. Pure space diversity exploits antenna element separation only to extract uncorrelated signals from the propagation channel.

The following figure 3.22 shows the layout of the commented array.

Figure 3.22: Space and pattern diversity schemes for vertically linearly polarized antennas at $d = 0.5\lambda$ (negligible mutual coupling).

Vertically linearly polarized scheme at $d = 0.35\lambda$ antenna separation (scheme 3.7.1.2)

This scheme is a 2x1 linear array of antennas separated $d = 0.35\lambda$ and vertically linearly polarized.

In this scheme the mutual coupling between antenna elements is large and hence this scheme is used to investigate the influence of the mutual coupling on the performance of such diversity schemes, when the antennas have a linear polarization oriented in the vertical direction.

The following figure 3.23 shows the layout of the commented array.

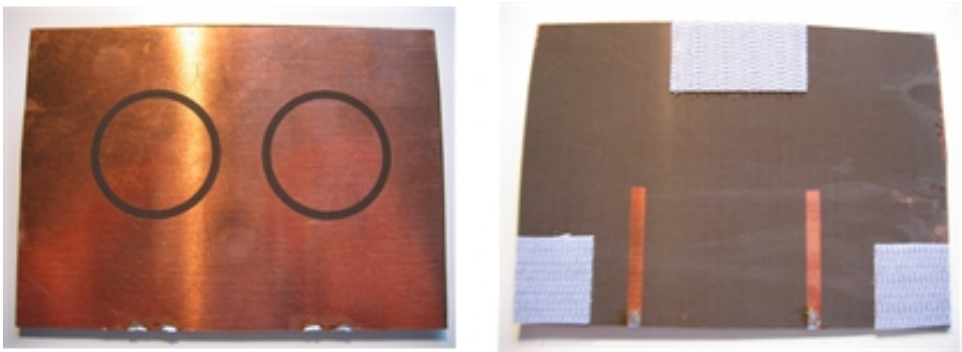

Figure 3.23: Space and pattern diversity schemes for vertically linearly polarized antennas at $d = 0.35\lambda$.

Horizontally linearly polarized scheme at $d = 0.5\lambda$ antenna separation (scheme 3.7.1.3)

Similarly to section 3.7.1.1, but with horizontally linearly polarized antennas.

The following figure 3.24 shows the layout of the commented array.

Horizontally linearly polarized scheme at $d = 0.35\lambda$ antenna separation (scheme 3.7.1.4)

Similarly to section 3.7.1.2, but with horizontally linearly polarized antennas.

The following figure 3.25 shows the layout of the commented array.

Figure 3.24: Space and pattern diversity schemes for horizontally linearly polarized antennas at $d = 0.5\lambda$.

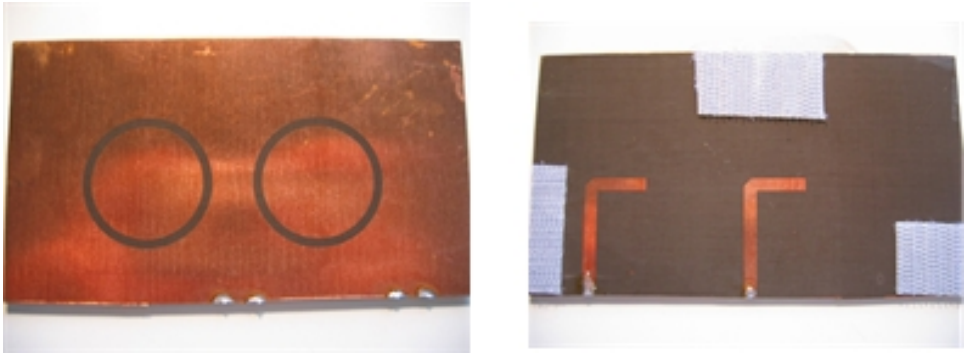

Figure 3.25: Space and pattern diversity schemes for horizontally linearly polarized antennas at $d = 0.35\lambda$.

Circularly polarized scheme at $d = 0.5\lambda$ antenna separation (scheme 3.7.1.5)

Similarly to section 3.7.1.1, but with circulaly polarized antennas.

The following figure 3.26 shows the layout of the commented array.

Circularly polarized scheme at $d = 0.35\lambda$ antenna separation (scheme 3.7.1.6)

Similarly to section 3.7.1.2, but with circulaly polarized antennas.

The following figure 3.27 shows the layout of the commented array.

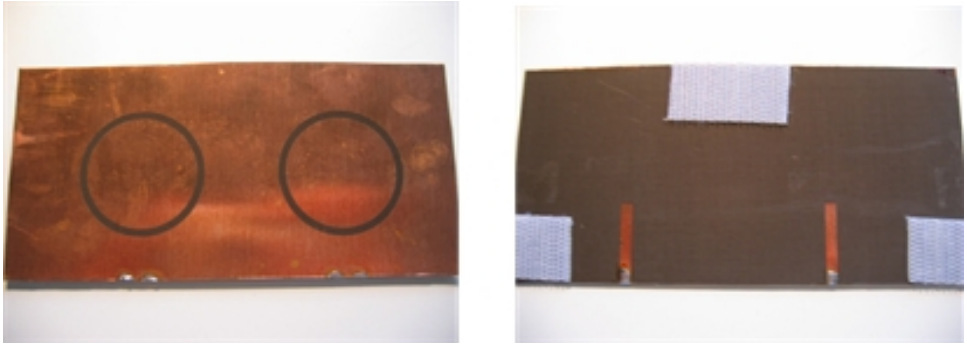

Figure 3.26: Space and pattern diversity schemes for circularly polarized antennas at $d = 0.5\lambda$.

Figure 3.27: Space and pattern diversity schemes for circularly polarized antennas at $d = 0.35\lambda$.

3.7.2 MEA schemes to investigate pure polarization antenna diversity

Vertical-Horizontal linearly polarized single antenna scheme

Pure polarization diversity exploits multiple antennas with different polarizations (linearly vertical and horizontal in our case) to obtain uncorrelated signals. The dual linearly polarized configuration of the ARSA was used on those schemes. Actually, there are two ways to study pure polarization diversity, by using one single antenna with multiple ports that can extract multiple polarizations, or by using several antennas, with different polarization. But in fact, this last approach is a combination

of spatial and polarization diversity. In our case, to study pure polarization diversity, one single antenna with two orthogonal polarizations was used, and the result compared with the 2x1 antenna array for pure space diversity. This scheme was designed to isolate the effects of space diversity from polarization diversity. Below, in figure 3.28 is presented the schematic for pure polarization diversity.

Figure 3.28: Scheme for pure polarization diversity.

The electrical characteristics of this configuration were presented previously when discussing about the dual polarized configuration for ARSA.

3.7.3 MEA schemes to investigate combined spatial and polarization antenna diversity

Those schemes combines two techniques of receiving diversity: space and polarization diversity. It uses antennas separated by a distance that is equal to the distance used on the space diversity scheme but in addition, it also introduces polarization diversity in a way that each adjacent antenna has a different polarization. In the literature, this is the typical configuration for polarization diversity, although actually is the inherent combination of two techniques. When combining space and polarization techniques, we can have single or dual polarized schemes. In any case, the orientation of the scheme is in the horizontal plane, to get the maxim advantage from multipath in terms of space diversity. However, the scheme has also been used vertically to study the level of polarization diversity of the channel, in the vertical and horizontal direction.

For single polarized schemes, one polarization is extracted from each antenna, while for the previous dual polarized scheme two orthogonal polarizations was extracted simultaneously.

Vertical-Horizontal linearly polarized scheme at $d = 0.5\lambda$ antenna separation (scheme 3.7.3.1)

This scheme is a 2x1 linear array of antennas separated $d = 0.5\lambda$ with one antenna vertically linearly polarized and the other horizontally linearly polarized.

In this scheme the mutual coupling between antenna elements is small, almost negligible and hence this scheme is used to investigate the performance of such diversity schemes with negligible mutual coupling.

The following figure 3.29 shows the layout of the commented array.

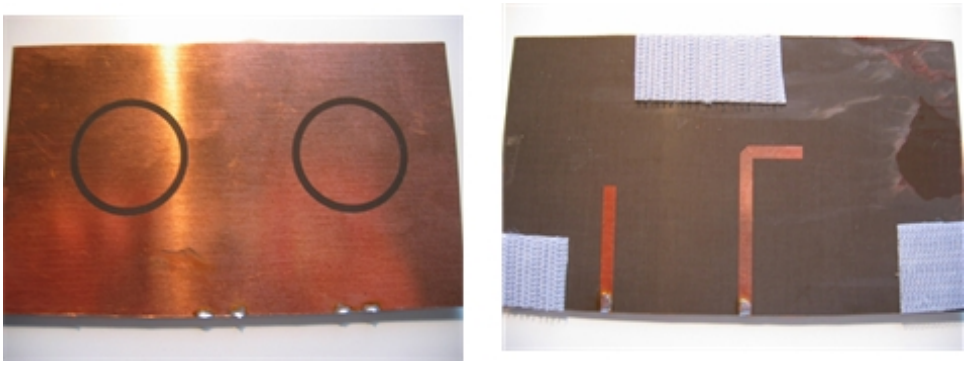

Figure 3.29: Combined spatial and polarization diversity schemes for linearly polarized antennas at $d = 0.5\lambda$.

Vertical-Horizontal linearly polarized scheme at $d = 0.35\lambda$ antenna separation (scheme 3.7.3.2)

Same as in 3.7.3.1 but with antennas separated $d = 0.35\lambda$.

In this scheme the mutual coupling between antenna elements is large and hence

this scheme is used to investigate the influence of the mutual coupling on the performance of such diversity schemes.

The following figure 3.30 shows the layout of the commented array.

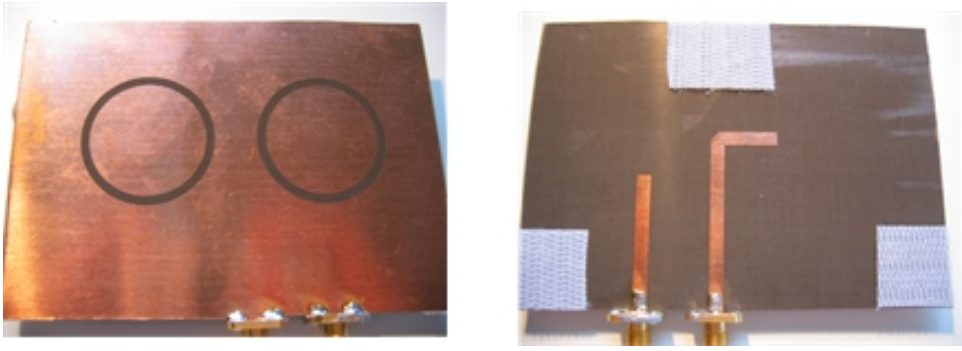

Figure 3.30: Combined spatial and polarization diversity schemes for linearly polarized antennas at $d = 0.35\lambda$.

Righ/Left Hand circularly polarized scheme at $d = 0.5\lambda$ antenna separation (scheme 3.7.3.3)

Same as in 3.7.3.1 but with antennas separated $d = 0.5\lambda$ and Righ/Left Hand circularly polarized antennas.

The following figure 3.31 shows the layout of the commented array.

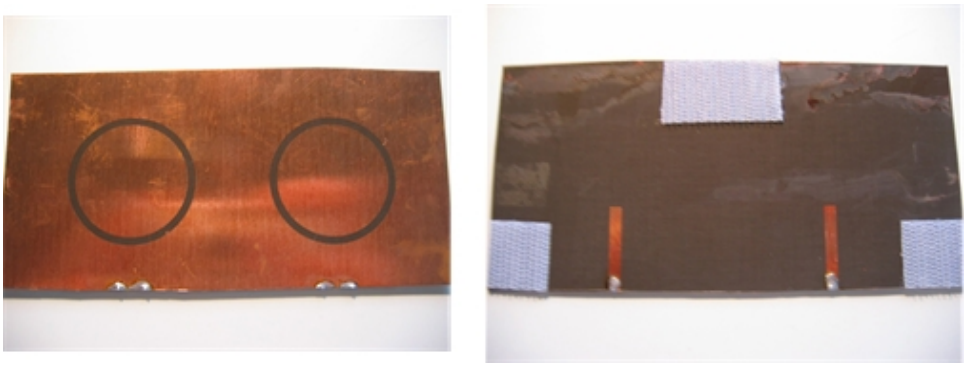

Figure 3.31: Combined spatial and polarization diversity schemes for circularly polarized antennas at $d = 0.5\lambda$.

Righ/Left Hand circularly polarized scheme at $d = 0.35\lambda$ antenna separation (scheme 3.7.3.4)

Same as in 3.7.3.2 but with antennas separated $d = 0.35\lambda$ and Righ/Left Hand circularly polarized antennas.

The following figure 3.32 shows the layout of the commented array.

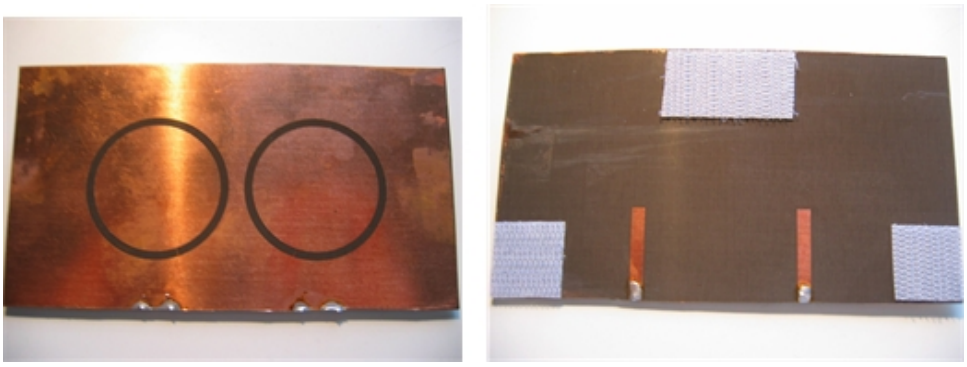

Figure 3.32: Combined spatial and polarization diversity schemes for circularly polarized antennas at $d = 0.35\lambda$.

3.8 MEA diversity schemes characteristics summary

Table 3.8 summarizes the main key electrical characteristics from the measurements and simulations for the antenna diversity schemes characteristics. Boards were fabricated on Rogers with h=1.1938 mm, $\epsilon = 2.5$, $\tan\delta = 0.0015$ and $t = 17\mu m$. On the table, $S_{21-MEAS}$ is the measured isolation between the ports of the array, $S_{21-HFSS9}$ is the simulated isolation with HFSS 9.0, θ_{MC} is the angle, from the vertical, at which the the radiation pattern of a single antenna element, deformated (steered) due to the effect of the mutual coupling, has a maximum of gain (in other words: in the absence of adjacent antennas or mutual coupling, $\theta_{MC} = 0$), G_{MC} is the peak gain of the radiation pattern under the influence of the mutual coupling and $HPBW_{MC}$ is

the Half-Power Beamwidht.

In all diversity schemes, smaller antenna separation accounts for larger mutual coupling (S_{21}). This produces the beam pattern of each individual antenna to steer towards its adjacent antenna.

The vertically linearly polarized (VLP) schemes (3.7.1.1 and 3.7.1.2) have 9.7 dB isolation between ports at $d = 0.35\lambda$, and 17.8 dB at $d = 0.5\lambda$. Compare to other schemes, the coupling is large and the reason is because at the closer distance the electric field is maximum and in phase.

The horizontally linearly polarized (HLP) schemes (3.7.1.3 and 3.7.1.4) provides 18 dB isolation between ports at $d = 0.35\lambda$ and 19 dB at $d = 0.5\lambda$. This polarization has small coupling because at the closer distance the electrical field is in phase but there is a minimum in magnitude.

Regarding the pattern deformation, however, for an antenna separation of $d = 0.35\lambda$, in the VLP scheme (3.7.1.2), each beam is steered by 17°, and for the HLP (3.7.1.4) scheme 21°. No steering is observed at $d = 0.5\lambda$ in both cases.

The circularly polarized (CP) schemes (3.7.1.5 and 3.7.1.6) have 17 dB isolation between ports at an antenna separation of $d = 0.35\lambda$, and 23 dB at $d = 0.5\lambda$. In this case, the small coupling is due to the electric field nature in circularly polarized schemes. Regarding the pattern deformation, at $d = 0.35\lambda$ each beam is steered by 26°, and 24° at $d = 0.5\lambda$.

On the other hand, regarding the schemes to study polarization diversity, the one employing linearly polarized antennas (VHLP) schemes (3.7.3.1 and 3.7.3.2) have around 20dB isolation between ports, at an antenna separation of $d = 0.35\lambda$, and 40 dB at $d = 0.5\lambda$. Very high isolation is achieved because in that case, at the position where the adjacent slots are the closer, the electric field at that position are orthogonal each other, so they can't couple. At $d = 0.35\lambda$, in the VHLP schemes the two antenna beams are steered asymmetrically by $-10°$ and 34° respectively, and similarly at $d = 0.5\lambda$.

In both, HFSS9 and measurements, the schemes (3.7.3.3 and 3.7.3.4) employing circularly polarized antennas (RLCP) has lower isolation between port to the CP scheme, around 17.7dB at $d = 0.35\lambda$ and 22 dB at $d = 0.5\lambda$. The lower isolation for circularly polarized antennas can be explained in this case by the fact that at the most close position between slots, the electric field for both slots, are in phase. However, in ADS simulations, those scheme has much more mutual coupling in both cases. The VLP scheme is the only one in which the isolation is below 15 dB at $d = 0.35\lambda$. All the schemes have an isolation between ports over 15 dB at $d = 0.5\lambda$.

In either schemes, the ones used to investigate spatial, pattern or polarization diversity, for both linearly and circularly polarized antennas, the mutual coupling steers antenna pattern beam, increasing individual gain and narrowing the individual Half power Beamwidht (HPBW).

In the case of pattern diversity, and for linearly and circularly polarized antennas, the mutual coupling degrades null depth for the combined beam and this is due to the deformation of each antenna pattern. The first to second lobe level (FSLL) is improved due to smaller spacing between antennas. Mutual coupling decreases total pattern gain and increases total HPBW, but it does not affect the direction of the combined beam.

CP schemes have lower mutual coupling than VLP or HLP schemes because the electric in the first case is out of phase and in the second case in in phase, although the beam steering angle due to mutual coupling is larger in CP schemes, for a fixed distance.

VHLP schemes are more sensitive to beam steering, due to mutual coupling, than VLP or HLP schemes. The beams are steered asymmetrically in the scheme VHLP. At both $d = 0.5\lambda$ and $d = 0.35\lambda$, VHLP scheme have $10°/30°$ beam steering. In RLCP scheme the angle is $15°$ and $30°$ respectively. All the schemes have $0°$ steering angle at $d = 0.5\lambda$.

For the vertical-horizontal linearly polarized single antenna scheme the two linearly polarized orthogonal polarizations have an isolation of 16 dB.

Table 3.1: Summary of the measurements and simulations for the antenna diversity schemes characteristics. Boards fabricated on Rogers with h=1.1938 mm, $\epsilon = 2.5$, $\tan\delta = 0.0015$ and $t = 17\mu m$

Antenna scheme	d	$S_{21-MEAS}$	$S_{21-HFSS9}$	θ_{MC}	G_{MC}	$HPBW_{MC}$
3.7.1.1	0.5λ	-17.8 dB	-23.1 dB	0°	3.7 dBi	94°
3.7.1.2	0.35λ	-9.7 dB	-13.5 dB	17.9°	3.9 dBi	80°
3.7.1.3	0.5λ	-19 dB	-17.5 dB	0°, ±24° (1.3dBi at 0°)	2.2 dBi	110°
3.7.1.4	0.35λ	-18 dB	-16.3 dB	21°	3 dBi	97°
3.7.1.5	0.5λ	-22.5 dB	-20 dB	24°	3.3 dBi	82°
3.7.1.6	0.35λ	-17 dB	-17.3 dB	26°	3.9 dBi	56°
3.7.3.1	0.5λ	-40 dB	-46.6 dB	V: $-10°$ H: 34°	V: 4 dBi H: 3.4 dBi	V: 85° H: 47°
3.7.3.2	0.35λ	-20 dB	-22.8 dB	V: $-12°$ V: 30°	V: 4.6 dBi V: 4.5 dBi	V: 48° V: 55°
3.7.3.3	0.5λ	-24 dB	-21 dB	15°	2.4 dBi	107°
3.7.3.4	0.35λ	-18.6 dB	-16 dB	30°	3.2 dBi	52°

After researching in how to improve the isolation characteristic of the schemes presented in this section, it was found that the schemes that provides better isolatin is the one in which the feeding lines are 45° rotated with respect the other configurations. Assuming that the first mode is excited, at the position in the slot where most close are the antennas, that is, at $\phi = -90°$ and $\phi = 90°$, the electric field in the slot, between adjacent antennas is not in phase, in contraposition when no rotation on the feed lines is used. Hence, the electric field cannot couple that easy as in the other schemes and better isolation and lower mutual coupling can be achieved. This scheme, however, provides 45 rotated linearly polarized antennas with respect to the other schemes; so actually, they are able to extract part of the vertical and horizontal component of the electric field coming from the channel, in contraposition with the other schemes that only can extract the vertical component.

It needs to be emphasized that although the circularly polarized antenna is larger ($l = 1.5\lambda$) than the linearly polarized antenna ($l = 1\lambda$), the distance between centers of antennas is always kept the same in all the schemes, because we are fixing the area (distance between antennas actually) as a main constrain.

Chapter 4

Experimental setup

On this section we will describe the experimental setup that was designed and fabricated in order to conduct the measurements regarding diversity techniques and schemes.

In previous research works, a previous experimental setup was used to conduct the receiving diversity experiments, however it was limited to measure up to 3 simultaneous incoming radio frequency (RF) signals, coming from the antennas. The system was adapted to conduct the measurements at the frequency of 2.45 GHz.

4.1 Mesurement setup description and design

The experimental setup is an RF circuitry that detects the power coming from each one of the antennas and stores the data in a file in the hard disk of a computer. We called "branch" to the circuitry that detects the RF power coming from one individual antenna. The experimental setup can have up to three branches to measure simultaneously the signal from three antennas. Each branch is made of a low noise amplifiers, followed by a band pass filter, and a power detector. The output of the power detector is passed to a power multimeter that digitalizes the data. After this,

the data is read by a computer that stores the information on a file, for later post processing and computation of the diversity parameters.

The low noise amplifier is in fact a high gain and high linearity power amplifier that amplifies the signal 30 dB. The power detector/sensor is from Agilent. It can detect a signal in the range of -70 dBm to 20 dBm within the frequency range that goes from 10 MHz to 18 GHz. The band pass filter was designed and fabricated on the laboratory because we obtained better performance, in terms of larger selectivity and lower insertion loss, than other chip based band pass filters, like the chip 2450BP41D100A from Johanson Technologies, but at the expenses of larger board area. To better represent the topology of the experimental setup, on the figure 4.1 we present a schematic of it.

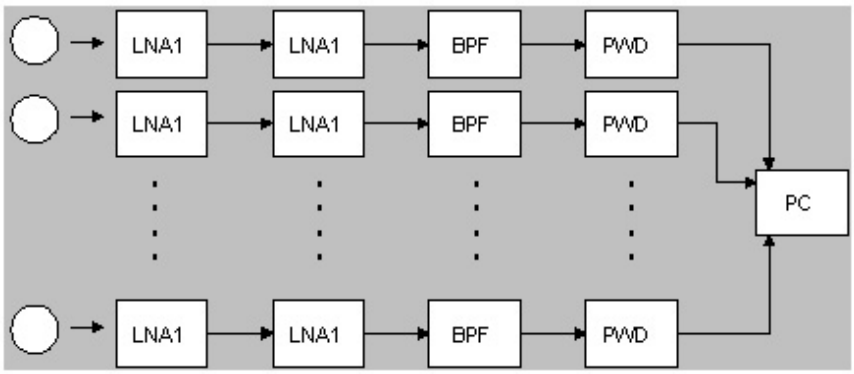

Figure 4.1: Schematic of the experimental setup: the circles represent the ARSA antennas.

As we can see on the schematic, a low noise amplifier is placed in the first two stages of the RF branches. It amplifies the signal coming from the antennas and is followed by a band pass filter that only allows passing the frequencies that are of interest to be detected on the power detector, which is in the last stage of the chain. The reason for placing the amplifiers before the band pass filter is to reduce to the maximum as possible the noise figure on the RF branch, and hence, increase sensitivity. On measurements, it was observed that if the band pass filter was placed before the amplifiers, this configuration was introducing much noise, that is, the power sensitivity was decreased, than in the configuration where the filter was placed after.

This has to do with the insertion loss of the filter component and connectors and is also predicted on the Friis formula, showed below:

$$NF_T = 1 + (NF_1 - 1) + \frac{NF_2 - 1}{Ap_1} + ... + \frac{NF_m - 1}{Ap_1...Ap_{m-1}} \tag{4.1}$$

This equation tells us that the first stages in a cascade are the most critical in terms of noise, because the noise contributed by each stage decreases as the gain preceding the stage increases. Components with moderate or large insertion loss should be avoided at the first stages, because the noise figure of those stages is amplified on the following circuit. As initially thought, when a narrowband lossy filter is interposed between the antenna and the low noise amplifier in a receiver to reject out-of-band interferers, the noise figure is increased and hence is better in terms of noise, to place the filter after the amplifiers.

The design of the overall experimental setup was conducted by using the ADS software from Agilent, because it provides a very powerful utility for RF systems design.

4.1.1 Overall specifications

The initial specifications for one branch were the following: cumulative gain of 30 dB, cumulative noise figure of approximately 4 dB, typical input dynamic range from -85 dBm to -50 dBm for a measured noise floor of -100 dBm. When choosing the components, the cascade IIP3 point and IP1 dB were verified to be inside the appropriate range for those components so that when connected all together, they can meet the requirements.

4.1.2 Substrate considerations

The substrate used to simulate and fabricate the experimental setup was Roger RO3006, which is a ceramic-filled PTFE composite with excellent electrical and me-

chanical stability, with dielectric constant e = 6.15 and thickness h = 0.63 mm. On this case, high dielectric constant and moderate thickness for the substrate is appropriate, for circuit compactness and microstrip lines with a width comparable to the chip pads dimensions. Substrate dielectric losses are still low enough for this application.

4.1.3 Band pass filter design

Two options for the band pass filter were considered: the first base on a chip filter (2450BP41D100A from Johanson Technologies) and the second based on a filter with couple lines. The initial specifications were: center frequency fo=2.45GHz, band-pass bandwidth of 100MHz, insertion loss of 0.1 dB and a selectivity of 35 dB at 400MHz from the center frequency. After hand design following the procedure described on [12] and simulation/optimization on ADS for both approaches, the filter with coupled lines was found to be more selective and provide lower insertion loss than the filter base on a chip. On the following picture 4.2 we present the simulation results for both approaches.

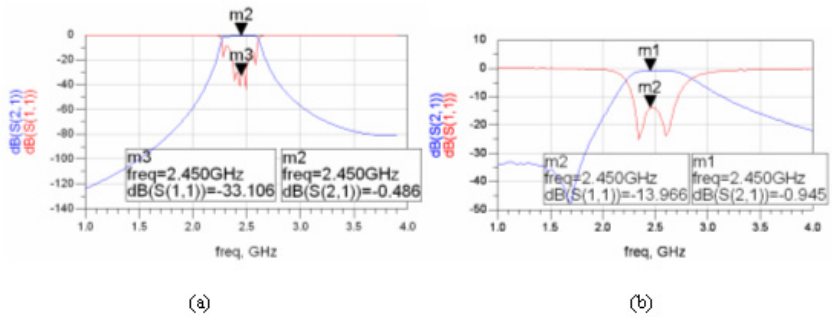

Figure 4.2: (a) Simulated return loss (m2) and insertion loss (m1) for the couple lines filter, (b) same data for chip based filter.

As we can see, when considering the losses of the real substrate, the initial specifications couldn't be meet, by keeping the same order for the filter, however they were still acceptable. From simulation, and for the coupled lines filter, the insertion loss is around 0.5 dB at the center frequency and the bandwidth is approximately 250MHz.

The return loss is -33 dB at the center frequency.

Figure 4.3 shows the measured return loss and insertion loss of the fabricated filter.

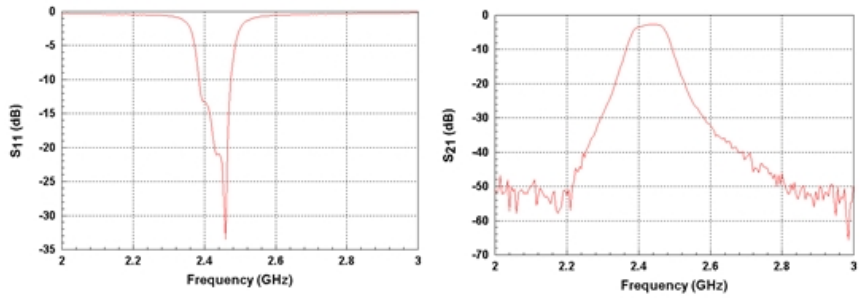

Figure 4.3: Measured return loss and insertion loss of the fabricated filter.

As seen, from measurements, the insert loss was 1.7 dB and the bandwidth around 250MHz. The differences in bandwidth may have to do with fabrication issues like over-etching, and the loss introduced difference with the attenuation introduced by the SMA connectors.

Figure 4.4 shows a picture of the band-pass filter once fabricated.

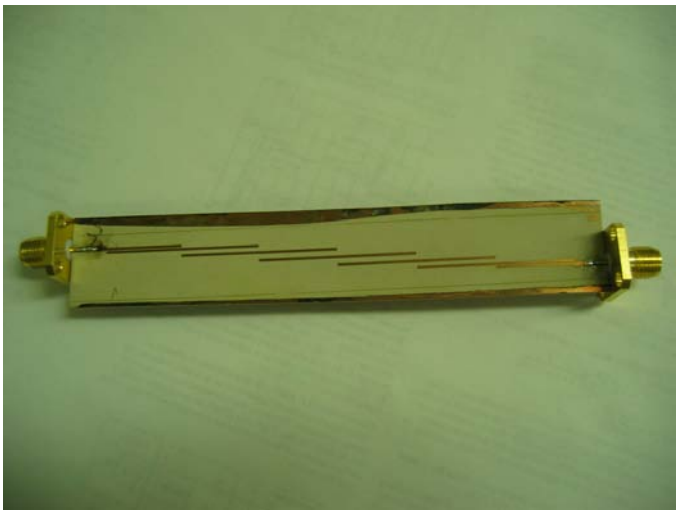

Figure 4.4: Picture of the fabricated 2.45 GHz band-pass filter.

4.1.4 Additional instruments for the experimental setup

For testing the performance of the fabricated components and branches, the following instruments were used: vector network analyzer 8510C from Agilent, TENMA power supply, FLUKE multi-meter, spectrum analyzer 8565E from HP, and synthesized CW generator 83712B from Agilent.

4.2 Description of the fabrication process

The experimental setup was fabricated in one of the laboratories of the RF Design and Characterization Group. The boards for the different components of the experimental setup, like the amplifiers, filters and the power detectors, were fabricated using standard board processing techniques. Later, all the necessary components were soldered. The antenna setups for the diversity schemes were fabricated using the same technique.

On the next lines the used board processing technique will be described. It has to be said that previous to the fabrications, some work need to be done on the drawing of the mask that later will be used on the process. Those mask are binary mask that are used to expose the photoresist only on the desired areas, in order to shape the desired circuit on the board.

On the next lines we summarize the recipe used for the board fabrication:

1. Clean the surface of interest on the board with Acetone, and later rinse it with water and dry with high-pressure air.
2. Spin the photoresist for about 30 seconds at 60V (2000 rpm). The photoresist chemical is AZ P4210.
3. Soft bake at 110 degrees for 3 minutes in the oven.
4. Let cold the board down.

5. Place the mask on the board and expose the photoresist for 5 minutes with Ultra-Violet (UV) light.

6. Develop the photoresist for 1 minute approximately. It's important to verify that the photoresist on the exposed region is completely gone. If not, the time needs to be extended. The developer chemical is AZ 400K.

7. Rinse the board with water and dry it with high-pressure air.

8. Hard bake at 110 degree for 10 minutes in the oven.

9. Protect the back plane of the board with blue scotch tape.

10. Heat the copper etching at 70-80 degrees and introduce the sample to etch on it. Leave it for 7-8 minutes approximately. The copper etchant chemical is Ferric Chloride.

11. Rinse with water and dry with high-pressure air.

Regarding this fabrication process it is important to remark several aspects. Fist, it was noticed that high temperature etching process, around 80C instead of 35C is favorable in terms of over-etching effect reduction since it was noticed that lower temperatures for etching take more time to etch the copper but at the same time the over-etching in certain parts of the circuit was larger. In any case, however, it was important to compensate the circuit for over-etching, at least on the parts were the distances were comparable to the over-etching. In our case, the band-pass filter was the only component to be compensated for this effect by making the metal structures around 20 mm larger in all the dimensions. One of the most critical parts in the process is when spinning the photoresist. Especially when the surface where the photoresist needs to be deposited is very large, like for the antennas, it's very important to make sure that the surface is enough clean and planar so that the photoresist is going to be deposited uniformly or at least in all the parts of the board. Another important step during fabrication is to make sure that all the photoresist that has been exposed to UV light is developed. To distinguish what parts still have some

photoresist, is a matter of experience, and normally if the surface has a metallic color means that the photoresist is correctly removed. Once the board has been fabricated is also important to clean the surface with Acetone. This is because having a layer of photoresist on the circuitry can modify the electrical behavior of transmission lines or the same circuit.

4.3 Digital signal processing setup

In order to obtain some relevant information from the measurements, it was needed a processing stage that recollects the data and computes the desired receiving diversity parameters.

In this sense, to evaluate the Rayleigh-fading statistics of the measured data, it was necessary first to extract the fast fading signal, due to the multipath phenomena, from the local mean signal level, corresponding to the slow fading. This fast fading has been proven to be Rayleigh distributed. Then, the received signal r(t) on an antenna channel can be expressed as follows:

$$r(t) = m(t) + f(t) \tag{4.2}$$

where f(t) is the fast Rayleigh-fading signal and m(t) is the local mean signal level, normally modeled as a lognormal signal. The signal m(t) is a slow variation and varies with distance r (distance from the emitter to the receiver) as a function of $log(\frac{1}{r^2})$ in rural environments and $log(\frac{1}{r^4})$ in dense urban areas. The Rayleigh-fading signal can be computed as follows:

$$f(t) = r(t) - m(t) = r(t) - \frac{1}{\Delta t}\int r(t)dt|_{\Delta t=(\frac{40\lambda}{v})} \tag{4.3}$$

where v is the velocity of the mobile terminal and Δt is the time required to travel a certain distance at that velocity. This distance has to be large enough to avoid that m(t) includes fluctuations due to fast fading, but it cannot be to large because in

that case, fluctuations in m(t) due to propagation loss over varying terrain would be averaged out. With the mean signal removed, the fast-fading signal varies about a zero reference and the probability of fading outages can be independently examined. Typically, this is plotted as a cumulative distribution function (CDF) of the fading signal f(t). The diversity gain performance is obtained by comparing the fading CDF of $f_i(t)$ on a single antenna channel at a specified probability to the fading CFD of $f_{div}(t)$, the fast fading associated with the combined diversity received output. We can express the CDF of $f_i(t)$ as:

$$CDF_i = P[X_i \leq x_0] \tag{4.4}$$

where X_i is the fade depths of $f_i(t)$, the random variable of CDF_i. We can express the CDF of $f_{div}(t)$ as:

$$CDF_{div} = P[X_{div} \leq x_0] \tag{4.5}$$

where X_{div} is the fade depths of $f_{div}(t)$, the random variable of CDF_{div}. Then the diversity gain $G_{div}(p_0)$ at the specified probability p_0 is expressed, in dB scale, as:

$$G_{div}(p_0) = X_{div}[P = p_0] - X_i[P = p_0]. \tag{4.6}$$

In the case of Selection Diversity (SD) as a diversity combining technique, and for space diversity schemes, the diversity gain is computed by comparing the fast fading CDF of a single antenna, with the fast fading CDF of the best antenna in terms of higher SNR. In the case of the pattern diversity schemes, the best antenna is considered in the sense of best direction of arrival, that is, it's normally compared the fast-fading component of the strongest beam at all times with the fast-fading component of a fixed beam. The strongest beam, over time, may come from different antenna beams as the maximum mobile received signal changes its direction of arrival. Another method to consider pattern diversity gain is to compare the strongest beam component signal with the signal coming from one individual antenna. In this research

both approaches have been considered. The first one is the traditional approach but we consider that the second approach is more convenient to really compare the performance with other diversity techniques that doesn't use group of antennas to create beams, like space and polarization diversity.

In our measurements, we assumed that an infinite speed could be used to switch between channels. In other words, the best signal among the channels was considered as an output of the system at all time. From those expressions, the diversity gain, and in addition the equations power imbalance and correlation coefficient were normally computed and plotted. Finally, a plot of the probability that SNR drops below a certain threshold for different assigned areas of the antenna for all the types of diversity (spatial, polarization and angle) and schemes, were produced.

In addition, other methods to take advantage of diversity were considered like the Maximal Ratio Combining (MRC) and Equal Gain (EG).

All those ideas and equation stated above that are used to compute the diversity gain, were programmed so that at this moment it is possible to directly compute, from the raw data coming from the measurements, all those parameters. This computerization was done in previous research works. The program was basically written in LabView and uses Matlab libraries to plot and computed the parameters.

4.4 Measurements discussion

The receiving diversity experiments were conducted by using the proposed diversity techniques and schemes in a rich scatter environment to evaluate the probability of the amplitude of the received signal falls below a certain power level versus the signal to noise ratio (SNR) for the best combined output signal, with SD, MRC or EG.

In our measurements, the transmitter was located in a room and the receiver, with the receiving diversity schemes installed on it, were displaced at a constant velocity in some other rooms, 50m away approximately from the transmitter. Rayleigh

distributions for the received signals were obtained. Normally, the transmitted power level was around 30 dBm and in reception the power level was oscillating from -80 dBm to -50 dBm, previous amplification.

When conducting the experiments, multiple measurements were conducted for the same diversity schemes under study, along a particular path. In addition, the experiments were conducted over several paths in order to have a more generic representation of the behavior of the diversity schemes. Figure 4.5 shows a map of the place where the experiments were conducted.

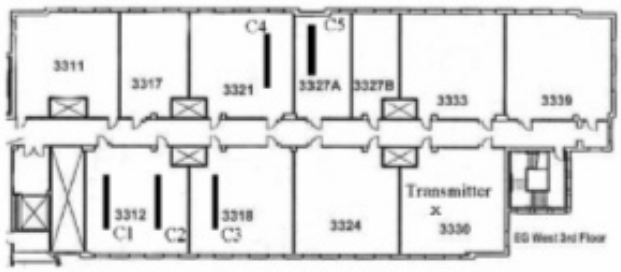

Figure 4.5: Floor plan of environment showing some of the used paths. The approximate total dimensions are 55m x 23m.

The devices involved in the measurement were, the antenna setups that constitute the diversity schemes under test, the experimental setup used to record the power coming from each one of the antennas, and a personal computer where the data was stored.

When conducting the measurements, the number of samples was important and the reason has already been commented previously when talking about the Δt parameter in the diversity gain computation. In our case, the numbers of samples per measurement were 1000, in a total of 2 minutes time.

Chapter 5

Results discussion

On this section we will present the results and conclusions obtained from the measurements and the study on receiving diversity techniques and the characterization of the indoor channel. The results here presented have been recently published by the author in [6].

5.1 Indoor channel characterization

The first measurements we did were to characterize the channel response of the propagation channel, in particular to determine: path losses, cross-polarization coupling and the fading. Different path losses accounts for differences in the transmission coefficients through walls. Depolarization losses or cross-polarization coupling accounts for the oblique reflections from walls and scattering from indoor clutter that produces coupling between orthogonal polarizations.

As commented before the floor plan dimensions were 55 m x 23 m and the operating frequency 2.45 GHz.

In our particular channel and regarding path losses, the horizontal polarization resulted in 3 dB less path loss than the vertical polarization. Right hand circularly

Table 5.1: Propagation path loss characteristics of each polarization in the indoor channel

Polarization at the TX	Polarization at the RX	Path loss
Vertical	Vertical	90 dB
Horizontal	Horizontal	87 dB
RHCP	RHCP	88 dB
LHCP	LHCP	89 dB
Polarization at the TX	Polarization at the RX	Coupling
Vertical	Horizontal	-2.2 dB
Horizontal	Vertical	-2.3 dB
LHCP	RHCP	-1.3 dB
RHCP	LHCP	-0.9 dB

polarized waves resulted in 0.7 dB less path loss than Left hand circularly polarized, hence showing almost the same propagation characteristics. The horizontal polarization resulted in 1 dB less path loss than Right hand circularly polarization and finally, the absolute path loss for the vertical polarization was approximately 90 dB. Next table summarizes the results:

The cross-polarization coupling was found to be -2.2 dB and -2.3 dB from vertical to horizontal and from horizontal to vertical polarizations respectively. It was found to be -1.3 dB and -0.9 dB from left to right and right to left circular polarizations respectively.

Finally, regarding the fading, circularly polarized (CP) showed slightly more fast fading than linearly polarized (LP) waves. That is, the normalized power at 10% probability for CP was from 10.5 dB to 11 dB. The normalized power at 10% probability for LP was from 9 dB to 9.5 dB.

During the measurement session, 78 measurements were conducted at a sampling rate of 200 samples per second, with M=2 in the receiver and N=1 antennas in the transmitter.

Table 5.2: Receiving spatial diversity gains using a linear array of ARSA antennas

Polarization TX	Polarization RX	Scheme orientation	Antenna separation	Gain
Vertical	Vertical	Horizontal	$d = 0.5\lambda$	6.75 dB
Vertical	Vertical	Horizontal	$d = 0.35\lambda$	5.75 dB
Vertical	Vertical	Vertical	$d = 0.5\lambda$	5.5 dB
Vertical	Vertical	Vertical	$d = 0.35\lambda$	6.25 dB
Horizontal	Horizontal	Horizontal	$d = 0.5\lambda$	7 dB
Horizontal	Horizontal	Horizontal	$d = 0.35\lambda$	6.2 dB
Horizontal	Horizontal	Vertical	$d = 0.5\lambda$	4.6 dB
Horizontal	Horizontal	Vertical	$d = 0.35\lambda$	4.95 dB
Circular	Circular	Horizontal	$d = 0.5\lambda$	6.15 dB
Circular	Circular	Horizontal	$d = 0.35\lambda$	6.2 dB
Circular	Circular	Vertical	$d = 0.5\lambda$	6.05 dB
Circular	Circular	Vertical	$d = 0.35\lambda$	5.5 dB

5.2 Benefits of pure spatial receiving antenna diversity

In this section we will summarize the results obtained in the investigation of diversity gain using spatial receiving antenna diversity schemes. As commented previously on the technical discussion chapter, the variables on this study were:

1. Distance between antennas: $d = 0.5\lambda$ and $d = 0.35\lambda$ in our case.
2. Type of polarization: linearly polarized and circularly polarized.
3. Scheme orientation: vertical plane and horizontal plane.

The next table summarize the results from the experiments. Table 5.2 shows the measured spatial diversity gains for different configurations.

From the figures and the measured diversity gains, those are the main conclusions:

1. Using linearly polarized antennas, smaller antenna separation degrades the diversity gain because the signals received in the antennas are more correlated.

2. There are not pure spatial diversity schemes for smaller antenna separations. When the antennas are closely located, the total diversity gain is a join contribution of spatial separation and pattern diversity due to the deformation of the radiation patterns of the antennas due to the mutual coupling.

3. Circular polarization is a preferred polarization choice for diversity gain reliability in front of scheme rotation at large antenna separations. As seen from the experiments, rotating the antenna schemes of linearly polarized antennas, produces large variations in the diversity gain.

4. Although circular polarization is more insensitive to rotations, linearly polarized antennas, when aligned, produce the maximum diversity gain, at large antenna separations.

5. Fixing the type of polarization to linearly polarized antennas, large antenna separation is desirable when the scheme is horizontally oriented, and smaller antenna separation when the scheme is vertically oriented. This can be explained by the fact the signal diversity in the vertical direction is much smaller than in the horizontal direction.

6. In general, the spatial diversity of the channel in the vertical direction is smaller than in the horizontal direction. This can be explained from the fact that in indoor environments has been seen that the signal arrives within very small elevation angles over the horizontal plane.

5.2.1 Influence of mutual coupling

It is also known in the literature, that the mutual coupling can introduce some benefits on the diversity gain because it distorts the radiation pattern of adjacent antennas, lowering the correlation coefficient between them. The mutual coupling in some other scenarios can in fact reduce the diversity gain due to an increase of the power imbalance between ports, due to the fact that the patterns may be deformated in a way that is not appropriate to the channel propagation conditions.

In all the schemes studied above, the inter antenna spacing was fixed to be either $d = 0.5\lambda$ or $d = 0.35\lambda$. The possible benefits in the diversity gain at $d = 0.35\lambda$ due to the mutual coupling are very small compared to the reduction on the diversity gain due to the fact that the antennas are more closely located and the propagation channels themselves are highly correlated already. The interest is in the fact that the answer is clear for space and polarization diversity, but the question if mutual coupling could result or not in a benefit for pattern diversity schemes, has not yet a clear answer. So, mutual coupling plays an important role on diversity performance, but needs further investigation.

In our case, we notice that given a fixed antenna separation, there is to ways to reduce the mutual coupling on the planar annular slot ring antenna (without external network):

1. By varying the inter-antenna separation, as it can be seen on the table above.

2. By varying the input feeding point in the slot, such as 45 rotation for linearly polarized antennas, on space diversity schemes. In general, that means that depending on the relative geometric position of one adjacent antenna with respect to the others, the mutual coupling is going to be different, that is: circular disposition of the antenna array instead of rectangular disposition may introduce some benefits from the mutual coupling perspective.

5.3 Benefits of pure polarization diversity

When fixing the number of antennas to one antenna, that is, by fixing the area of the schemes to the area occupied by one single antenna, polarization diversity by itself allows us to exploit diversity, that is, it allows us to access to a higher number of uncorrelated channels. The benefits from pure polarization are a diversity gain of 5 dB for MRC as a combining technique. Previously, figure 3.9 showed the schematic used to study the benefits from pure polarization diversity.

We would like to make an special remark to the fact that in future research it would be very important to investigate which angle rotation between polarizations is necessary to consider that both polarizations are enough uncorrelated, in a wireless channel, or which is the optimum number of rotated polarizations that need to be extracted simultaneously. This knowledge would provide us with a rule of thumb in designing future re-configurable polarization based schemes. That is, to obtain a function that give us the correlation between two different polarizations as a function of its separation angle (rotation).

Those results tell us, again, the potential of polarization diversity on future re-configurable schemes. As we can see, for this particular case with two ports, polarization diversity is the most compact scheme but on the other hand it provides almost the highest diversity gain, together with spatial diversity.

5.4 Benefits of combining spatial and polarization diversity

In this section we will summarize the results obtained in the investigation of diversity gain using combined spatial and polarization receiving antenna diversity schemes. As commented above, the variables on this study were again:

1. Distance between antennas: $d = 0.5\lambda$ and $d = 0.35\lambda$ in our case.
2. Type of polarization: linearly polarized and circularly polarized.
3. Scheme orientation: vertical plane and horizontal plane.

The next table summarize the results from the experiments. Table 5.3 shows the measured spatial diversity gains for different configurations.

From the figures and the measured diversity gains, those are the main conclusions:

Table 5.3: Receiving polarization diversity gains using a linear array of ARSA antennas

Polarization TX	Polarization RX	Scheme orientation	Antenna separation	Gain
Vertical	Dual (V - H)	Horizontal	$d = 0.5\lambda$	4.8 dB
Vertical	Vertical	Horizontal	$d = 0.5\lambda$	6.2 dB
Vertical	Vertical	Horizontal	$d = 0.35\lambda$	5.8 dB
Vertical	Vertical	Vertical	$d = 0.5\lambda$	5.2 dB
Vertical	Vertical	Vertical	$d = 0.35\lambda$	4.8 dB
Horizontal	Dual (V - H)	Horizontal	$d = 0.5\lambda$	5.4 dB
Horizontal	Horizontal	Horizontal	$d = 0.5\lambda$	5.25 dB
Horizontal	Horizontal	Horizontal	$d = 0.35\lambda$	5 dB
Horizontal	Horizontal	Vertical	$d = 0.5\lambda$	4.95 dB
Horizontal	Horizontal	Vertical	$d = 0.35\lambda$	5.4 dB
Circular	Dual (V - H)	Horizontal	$d = 0.5\lambda$	5.6 dB
Circular	Circular	Horizontal	$d = 0.5\lambda$	5.75 dB
Circular	Circular	Horizontal	$d = 0.35\lambda$	6.25 dB
Circular	Circular	Vertical	$d = 0.5\lambda$	6.25 dB
Circular	Circular	Vertical	$d = 0.35\lambda$	6.1 dB

1. There are not pure polarization and spatial diversity schemes for smaller antenna separations. When the antennas are closely located, the total diversity gain is a join contribution of spatial separation, polarization and pattern diversity due to the deformation of the radiation patterns of the antennas due to the mutual coupling.

2. The combined spatial and polarization diversity gain, in our case, was in general smaller than the diversity gains using only spatial diversity, for linearly polarized antennas. This can be explained by the fact that when using polarization the power imbalance is larger due to different path and polarization losses. However, similar gains are obtained in the case of circularly polarized antennas.

3. Circular polarization is a preferred polarization choice for diversity gain reliability in front of scheme rotation at large antenna separations. As seen from the experiments, rotating the antenna schemes of linearly polarized antennas, produces large variations in the diversity gain. In addition, using circularly

polarized antennas produces the maximum diversity gain, compared to linearly polarized antennas.

4. In general, the polarization diversity of the channel in the vertical direction is smaller than in the horizontal direction. This can be explained from the fact that in indoor environments has been seen that the signal arrives within very small elevation angles over the horizontal plane.

5.4.1 Influence of polarization

It was interesting to notice that when the polarization of the transmitted was fixed to be linear, and the schemes at the received were changed from linearly polarized to circularly polarized, almost the same diversity gain was obtained. This fact tell us that due to the propagation of the signals on the channel, an due to its reflections and refractions, the distribution of the polarizations at the receiver is in such a way that the signals is insensitive to what kind of the polarization the receiver is using. And this is true, because in fact, linear polarization diversity and circular polarization (CP) diversity, in some sense, they both exploit two orthogonal polarizations, so that the received signal, since is no longer linearly polarized, "sees" the same scheme. In addition, if CP is used on the polarization diversity schemes, and the transmitter is either changed from linearly to circularly polarized, the same gain is obtained. This is again explained by the fact that, the multiples replicas of the signal, in their way from the transmitter to the receiver, that arrive at the receiver have multiple polarizations, and any polarization diversity schemes can take advantage of this, independently of what kind of polarization is being used for transmitting.

5.4.2 Influence of power imbalance and correlation coefficient

In all the tested schemes the correlation coefficient between the combined branches was very small, lower than 0.15, but on the other hand, the power imbalance be-

tween the most separated branches was always very large around 2-3 dB for adjacent branches.

5.5 Benefits of combining spatial and pattern diversity

In this section we will summarize the results obtained in the investigation of pattern diversity gain using receiving antenna diversity schemes. As in the other cases, the variables on this study were again:

1. Distance between antennas: $d = 0.5\lambda$ and $d = 0.35\lambda$ in our case.
2. Type of polarization: linearly polarized and circularly polarized.
3. Scheme orientation: vertical plane and horizontal plane.

The next table summarize the results from the experiments. Table 5.4 shows the measured spatial diversity gains for different configurations.

From the figures and the measured diversity gains, those are the main conclusions:

1. When the mutual coupling increases, in general degrades pattern diversity performance.
2. Non of the polarization is robust in front of signal degradation due to the rotation of the antenna scheme, from vertical to horizontal. However, the signal variation using linearly polarized antennas is much larger than using circularly polarized antennas. Linearly polarized antennas are preferred for larger diversity gains.
3. Horizontal orientation produces larger diversity gains than vertically oriented schemes. This can be explained by the fact that the signal diversity in the

Table 5.4: Receiving pattern diversity gains using a linear array of ARSA antennas

Polarization TX	Polarization RX	Scheme orientation	Antenna separation	Gain
Vertical	Vertical	Horizontal	$d = 0.5\lambda$	6.75 dB
Vertical	Vertical	Horizontal	$d = 0.35\lambda$	5.75 dB
Vertical	Vertical	Vertical	$d = 0.5\lambda$	5.5 dB
Vertical	Vertical	Vertical	$d = 0.35\lambda$	6.25 dB
Horizontal	Horizontal	Horizontal	$d = 0.5\lambda$	7 dB
Horizontal	Horizontal	Horizontal	$d = 0.35\lambda$	6.2 dB
Horizontal	Horizontal	Vertical	$d = 0.5\lambda$	4.6 dB
Horizontal	Horizontal	Vertical	$d = 0.35\lambda$	4.95 dB
Circular	Circular	Horizontal	$d = 0.5\lambda$	6.15 dB
Circular	Circular	Horizontal	$d = 0.35\lambda$	6.2 dB
Circular	Circular	Vertical	$d = 0.5\lambda$	6.05 dB
Circular	Circular	Vertical	$d = 0.35\lambda$	5.5 dB

vertical plane is much smaller than in the horizontal plane because the waves normally arrive to the receiver within small elevation angles and large angular spreads over the horizontal plane.

4. Pattern diversity provide similar levels of diversity gain than spatial diversity for linearly polarized antennas. Lower gains are obtained in the case of circularly polarized antennas. The fact that angular diversity provides similar gains than spatial diversity can be explained because our experiments were conducted in an indoor environment and on those type of environments, the diversity gain is very insensitive to the shape of the radiation pattern of the antennas as long as they cover the same area of the three-dimensional space. The true advantage of pattern diversity schemes over spatial diversity schemes is in line-of-sight environments, due to the fact that directional patterns of the antennas increase the combined signal to noise ratio.

5.5.1 Influence of mutual coupling

The benefits of mutual coupling on this diversity schemes are now more understood. As seen from the experiments, the mutual coupling in general degrades the resultant diversity gain because in general the mutual coupling correlates the generated beams by making them to overlap and loosing their directivity.

5.6 Previous research results

Receiving diversity techniques have already been studied from several years ago and much literature can be found in the international community. On the following lines we summarize the state-of-the-art on this field.

When studying diversity techniques one has to distinguish between diversity techniques designed to be operated on the base station from the ones designed to be operated on the mobile station. On the base station, although limited, there are not as many concerns regarding the total area occupied by the antenna system or the number of antennas used by the diversity schemes as in the mobile station.

Up to this moment, most of the diversity techniques have been based on its application on the base station, due to cost and space issues. However, some research has already been done for the application of those techniques on the handset terminal. In particular, this project focused on its applications for handset terminals although the results could also be extended for its use in base-stations. In addition, it has to be notice that the traditional ways for improving diversity on the transmitting side by placing largely separated antennas, is being replaced by closely spaced antennas in conjunction with space-time coding, allowing for transmitting and receiving diversity schemes at both the transmitter and the receiver.

Focusing on diversity techniques intended to be used on the base station, so that a large number of antennas can be used and they can be largely separated if necessary, angle and space diversity have been studied in different mobile radio environments.

The results indicate that pattern diversity compares closely with traditional space diversity in a complex scattering or dense urban location. However, for rural applications, pattern diversity does not work as effectively as space diversity. The main reason for the degraded angle-diversity performance in rural locations is a large mean-signal imbalance on the diversity channels. This difference in mean signal reduces the selection diversity gain on the order of that imbalance. Angle and space diversity reduce fading outages in an urban mobile radio environment where the propagation channel experiences Rayleigh-fading. However, less improvement is obtained in rural environment where the propagation channel has a dominant path and is better described by a Ricean fading.

Focusing on diversity techniques for its use on the handset terminal, where the antennas are normally very closely distributed compared to a base station, it has been shown that spatial, polarization and pattern diversity configurations performs different depending on the environment: LOS, NLOS, indoor or outdoor channels. Some of these important results have already been discussed when describing the spatial, polarization and pattern diversity techniques, in previous chapters of this thesis, so they won't be included again in this section but the reader can refer to them for further information. However, as a summary, the Clarke formula, on [3], that predicts the correlation for a given space between antennas in general predicts larger values than in reality. The reason is because this formula doesn't take into account the mutual coupling between the antenna elements at a given distance. It has been noticed that the correlation between the envelopes of signals received by two antennas is decreased if the patterns of each antenna are different. This is because the relative amplitudes of the incident multipath signals are different at each antenna, even if the antennas are collocated. And the reason why the patterns of closely spaced antennas that are omnidirectional in free space are distorted is due to the mutual coupling. On the other hand, for distances enough large so that the mutual coupling can be considered negligible, its true that the larger the separation the lower the correlation. So, for small distances where the mutual coupling is still strong, the measured envelope correlation for spatial diversity configurations is normally lower

than predicted by simple theory. This effect is caused by distortion of the individual antenna patterns due to mutual coupling and non-uniformity in the multipath angle of arrival. The effects of mutual coupling are not entirely beneficial, since the distorted patterns also cause power imbalance if the multipath is not uniformly distributed in angle. This reduces diversity gain compared to the gain that can be achieved using omnidirectional elements with a similar correlation coefficient.

In addition, it has also been observed that small variations (from 0.3l to 0.5l) on the vertical position of the antennas, the correlation remains almost invariant compared to the same separation for schemes totally horizontal. This is consistent with the assumption that multipath components are confined within a narrow range of elevation angles about horizontal.

It has been also proven that that the correlation between antennas on space diversity schemes, depends on the angle spread and the existence or not of a dominant path. In this sense it has been proven that in indoor channels the correlation is in general lower than in outdoor NLOS or even higher in outdoor LOS. The fact that lower correlation values can be achieved means that for the space diversity configurations, the antennas can be placed more closed one from the other by keeping the same performance. In LOS environments, where there exists a predominant signal component, the Ricean distribution models better the envelope of the received signal. For Ricean fast-fading channels, fading is less severe and the potential diversity gain is lower than in the Rayleigh fading channel. For NLOS environments like indoor and outdoor-to-indoor channels, the fading approaches the Rayleigh distribution, and multipath can be expected to be more evenly distributed than in the other case, so low envelope correlation for spatial configurations results. In general, diversity depends on correlation and power imbalance, but at the same time those two parameters depends on angle spread uniformity and the degree of predominant component.

In space diversity it was noticed that the power balance varied as a function of antenna spacing. The statistics for all type of channels were similar and the values of power imbalance were relatively large. This suggests that the assumption of perfectly uniform angular distribution of the multipath is not satisfied in most of the channels.

However, for large spacing, that is, larger than 0.25l, the power imbalance is always small.

Antenna diversity is most effective in flat fading channels, which affect the signal the same way over its bandwidth. Flat fading occurs in narrow-band systems with propagation distances of up to several kilometers and in wide-band systems over indoor and pico- or micro-cellular channels with small delay spreads.

Chapter 6

Conclusion

Receiving diversity techniques, thought SIMO communications schemes, can improve the average quality of the received signal in a wireless network. The extension of this work toward MIMO communication schemes is the key for future improvement on the performance of wireless communication systems and reconfigurable schemes. Antenna miniaturization and reconfigurable polarization-receiving diversity seems to the one of the most promising techniques to provide high diversity gains while preserving small antenna system dimension. Reconfigurability has been proven to be an important solution for cheap and simple receiving diversity schemes with near optimum performance at all times. On the other hand, it has been seen that the diversity performance is a complex phenomena that strongly depends on both the channel characteristics and the antenna scheme characteristics. There exist prefered polarizations and types of diversity among different configurations.

Chapter 7

Relevance to the telecommunication industry

The key factor for many California industries to be on the cutting edge of wireless technology depends heavily on the use of novel techniques upon their availability. Novel techniques allow the production of higher performance wireless systems at equivalent or lower cost compared to what are currently available. The use of receiving diversity combining will provide more reliable communications in the mobile wireless communication environment. The research developed on this project helped this technology to be available by investigation the selection of an optimal antenna configuration to take the maximum advantage of a diversity combining scheme with the minimal space used for the antenna systems. A successful exploitation of the wireless channel diversity can impact a mobile network in several ways. Reduced power requirements can result in increased coverage or improved battery life. Also reduced fade margins directly translate to better reuse factor and hence, increased system capacity.

Chapter 8

Future work

First, it needs to be said that in several parts of this thesis there are references to future works regarding some specific areas on receiving diversity techniques that will need to be further studied. However, in order to not repeat them again, the reader can found those references on previous chapters of the thesis.

This is a summary of some other future researches on this area:

1. Incorporate electromagnetic diversity aspects, like: polarization, antenna separation (mutual coupling) or radiation pattern; on transmitting diversity and see how they interact with space-time coding aspect. The reason is because until this moment transmitting diversity doesn't take into account those electromagnetic aspects. That is, firstly, spatial, polarization and pattern diversity (beamforming) have not been taken into consideration into a transmitting diversity scheme and it would be interesting to investigate this area. Secondly, it would also be interesting to study the benefits from sectored transmitting diversity schemes versus traditional omnidirectional and non-sectored transmitting diversity schemes. The goal is to study the benefits from having knowledge of the position of the mobile station on transmitting diversity schemes. Thirdly, we propose to study the benefits from using several beams pointing at different

directions inside the sector and compare it with the scheme on the first approach, that is, using several beams pointing at the same direction inside the sector. On the first, approach, all the employed beams covers the entire sector, while in the second approach, the beams only cover a region inside the sector. The goal is to go one step further than does communication theory, and investigate if this configuration may introduce some benefit. Is not intuitively how this configuration may perform. The common goal of all those approaches is to combine the knowledge provided by communication theory and electromagnetism theory, for better antenna design.

2. Incorporate receiving diversity conclusions (polarization diversity advantages) into the design of future re-configurable antennas and diversity schemes, for both transmitting and receiving.

3. Study the benefits from receiving diversity directly applied to a transmitting scheme (without involving transmitting diversity techniques or space time coding).

4. Complement this experimental work with and algebraic/analitical study of the commented phenomenas.

5. Implement a simulation tool to agilize study on diversity and compare the analitical, simulated and experimental results.

Bibliography

[1] L. Accatino, A. Angelucci, and B. Piovani. Design of butler matrices for multiport amplifier applications. *Microwave Engineering Europe*, pages 45–50, Apr 1992.

[2] J. Butler and R. Lowe. Beam forming matrix simplifies design of electronically scanned antennas. *Applied Superconductivity, IEEE Transactions on*, 9:170–173, Apr 1961.

[3] R. H. Clarke. A statistical theory of mobile-radio reception. *Bell Syst. Tech. Journal*, pages 957–1000, Jul 1968.

[4] Alonso Corona and M. J. Lancaster. A high-temperature superconducting butler matrix. *Applied Superconductivity, IEEE Transactions on*, 13(4):3867–3872, Dec 2003.

[5] G. Foschini and M. J. Gans. On limits of wireless communications in a fading environment when using multiples antennas. *Wireless Personal Communications*, 6:331–335, 1998.

[6] A. Grau, Sunan Liu, B.A. Cetiner, and Franco De Flaviis. Investigation of the influence of antenna array parameters on adaptive MIMO performance. *Antennas and Propagation, IEEE Transactions on*, 2:1704–1707, Jun 2004.

[7] M. Kavehrad and P. J. Mclane. Performance of low-complexity channel coding and diversity for spread spectrum in indoor, wireless communications. *ATT Technical Journal*, 64(8), Oct 1985.

[8] Young-Soon Lee, Ikmo Park, and Chull-Chai Shin. A miniaturized wilkinson power divider. *SANG-TAE KIM.*

[9] H. Levine and C. Papas. Theory of the circular diffraction antennas. *Antennas and Propagation, IEEE Transactions on*, 22(1):29–43, Jan 1951.

[10] P. Mastin and B. Rawat. Design of microstrip annular slot for mobile communications. *Antennas and Propagation, IEEE Transactions on.*

[11] H.J. Moody. The systematic design of the butler matrix. *Antennas and Propagation, IEEE Transactions on*, 12(6):786–788, Nov 1964.

[12] David M. Pozar. *Microwave Engineering.* John Wiley and Sons Inc., 2nd edition, 1998.

[13] Cheuk yu Edward Tong and Raymond Blundell. An annular slot antenna on a dielectric half-space. *Antennas and Propagation, IEEE Transactions on*, 42(7), Jul 1994.